ARTICLE OPEN



Chronic social isolation-unpredictable stress induces early-onset cognitive deficits and exacerbates AB accumulation in the 5xFAD mouse model of Alzheimer's disease

© The Author(s) 2025

Aging and genetic predisposition are the primary risk factors for Alzheimer's disease (AD), while chronic stress represents a modifiable risk factor that can accelerate aging and drive AD progression. However, the complex interplay between aging, chronic stress and genetic underpinnings in AD pathogenesis remains poorly understood. Notably, cognitive phenotyping in AD mouse models has yielded inconsistent results. In this study, we characterized the age-dependent trajectory of phenotypes in 5xFAD mice on a congenic C57BL/6 J background. These mice harbor five familial AD (FAD)-related mutations in the amyloid precursor protein (APP) and presenilin 1 (PSEN1) genes. Aβ plaque deposition was detected in specific brain regions by 4 months of age, but cognitive performance remained intact at this stage. However, by 8–9 months, these mice developed impairments in spatial working memory, novel object recognition memory, and social recognition memory. By 11 months, they also showed metabolic alterations, including lower body weight, higher energy expenditure and increased locomotor activity. Furthermore, after 10 days of chronic social isolation-unpredictable stress, 4-month-old 5xFAD mice exhibited cognitive deficits, accompanied by increased Aβ accumulation in the medial prefrontal cortex, hippocampus, and entorhinal cortex. In contrast, age- and sex-matched wild-type littermate controls subjected to the same stress paradigm showed no significant cognitive changes. These observations suggest that Aβ deposition increases stress vulnerability in 5xFAD mice. We conclude that the phenotypic expression of AD-related gene mutations, including pathological changes and cognitive decline, progresses with age and can be induced by chronic psychological stress, underscoring the interactive effects of stress, aging, and genetic vulnerability on disease onset and severity.

Molecular Psychiatry (2025) 30:4720-4735; https://doi.org/10.1038/s41380-025-03067-0

INTRODUCTION

Alzheimer's disease (AD) is a neurodegenerative disorder that causes progressive cognitive decline. It is the most common form of dementia, accounting for 60-80% of all dementia cases. Pathologically, AD is defined by the deposition of β -amyloid (A β) peptides in extracellular senile plaques and the presence of tau filaments in intracellular neurofibrillary tangles in the brain. Age is the greatest risk factor for developing AD. As a result, AD can be classified into two subtypes based on the age of onset. Early-onset AD (familial AD) occurs before age 65, accounting for approximately 1–6% of cases; late-onset AD (sporadic AD) develops at or after age 65, comprising about 95% of cases [1]. These subtypes differ not only in age of onset but also in their genetic underpinnings, influencing disease progression.

Mutations in the amyloid precursor protein (APP) [2, 3], presenilin 1 (PSEN1) [4, 5], and presenilin 2 (PSEN2) [6] genes, have been identified as major causes of familial, early-onset AD. APP encodes the A β precursor protein, which is processed by the sequential cleavages of β -secretase and γ -secretase to produce A β protein. PSEN1 and PSEN2 encode the presenilins, the catalytic subunit of the γ -secretase complex. Mutations in human APP, PSEN1 or PSEN2 genes result in overproduction of pathological A β

fragments, leading to the aggregation and formation of AB plaques. These mutations have been used to generate animal models for studying AD over the past few decades. Among transgenic mouse models of AD, the 5xFAD mouse model, coexpressing human APP and PSEN1 transgenes harboring five familial AD-linked mutations [7], has been widely used to recapitulate AD-related phenotypes [7]. However, originally established on a hybrid C57BL/6/SJL background [7], these mice inherit a combination of genes from both parental strains. This genetic heterogeneity can influence phenotypic variability, leading to complex gene-gene interactions that may impact disease progression and behavioral outcomes. Additionally, the SJL/J strain carries the retinal degeneration allele *Pde6b*^{rd1}, which can result in progressive retinal degeneration due to the loss of *Pde6b* function [8]. This degeneration may impair visual function and potentially confound behavioral assessments that rely on visionbased tasks, such as maze tests, object recognition tasks and social recognition tests. These genetic and phenotypic factors may contribute to variability in experimental outcomes, particularly in behavioral phenotypes [7, 9-11]. These caveats can be addressed by using 5xFAD mice on the congenic C57BL/6 strain background, in which the retinal degeneration allele Pde6brd1 has been bred

¹Department of Neuroscience & Regenerative Medicine, Medical College of Georgia at Augusta University, Augusta, GA, USA. [™]email: ylei@augusta.edu; xylu@augusta.edu

out of the strain and genetic differences outside the target region is minimized [12, 13]. Recently, several studies have characterized the phenotypic expression of this congenic C57BL/6 5xFAD line [14–16]. While AB pathology is largely consistent across studies, discrepancies exist in cognitive behavioral phenotypes. Notably, certain limitations in control group selection and behavioral testing methodologies may affect the interpretation of cognitive outcomes in these studies. For instance, Locci et al. [14] used the same wild-type control group for three different AD mouse models—APP^{NLGF} knock-in, 5xFAD, and APP/PS1 mice. Additionally, studies by Forner et al. [16] and Oblak et al. [15] relied on a single cognitive behavioral test and reported no cognitive phenotype in 5xFAD mice. Although cognitive impairment emerges later in the disease process, it remains a critical component for the clinical diagnosis of AD [17]. Therefore, further characterization of the progression of the cognitive decline in 5xFAD mice in relation to $A\bar{\beta}$ deposition is needed.

Chronic stress is a modifiable risk factor for AD, accelerating aging as well as the onset and progression of the disease [18-21]. Evidence suggests these effects are largely mediated through dysregulation of the hypothalamic-pituitary-adrenal (HPA) axis, resulting in increased glucocorticoids [22-26]. However, the impact of chronic stress on neuropathological processes and cognitive decline in AD remains poorly understood. We have previously employed a chronic unpredictable stress paradigm in socially isolated mice to induce cellular, neuroendocrine and behavioral changes, effectively modeling aspects of human neuropsychiatric conditions [27–30]. In this study, we characterized cognitive phenotypes in 5xFAD mice at different ages using behavioral tests targeting distinct cognitive domains. Additionally, we assessed age-dependent neuropathological and metabolic changes to explore their temporal relationships with cognitive decline. Furthermore, we investigated the impact of chronic social isolation-unpredictable stress on cognitive performance and $\ensuremath{\mathsf{A}}\ensuremath{\beta}$ accumulation in young 5xFAD mice to determine whether prolonged psychological stress induces or exacerbates phenotypic expression.

MATERIALS AND METHODS

Animals

Hemizygous transgenic 5xFAD mice on a congenic C57BL/6J background (Stock No # 034848-JAX) were obtained from the Mutant Mouse Resource and Research Center (MMRRC). These mice express human APP and PSEN1 transgenes with a total of five familial AD mutations, including the Swedish (K670N/M671L), Florida (I716V), and London (V717I) mutations in the APP gene, and the M146L and L286V mutations in the PSEN1 transgene [7]. The expression of both transgenes is driven by the neuron-specific Thy1 promoter [7]. Male hemizygous transgenic 5xFAD mice were crossed with female wildtype (WT) C57BL/6J mice (Stock No #000664) to maintain the 5xFAD and nontransgenic WT colonies. All offspring were genotyped for both the APP and PSEN1 transgenes using DNA extracted from tail snips as a template for PCRbased analysis using the following primers: common forward, 5'-ACCCCCATGTCAGAGTTCCT-3'; mutant reverse, 5'-CGGGCCTCTTCGCTATTA C-3'; wild-type reverse: 5'-TATACAACCTTGGGGGATGG-3'. Mice were housed in groups of 3-5 mice per individually ventilated cage, with ad libitum access to food and water under a 12-h light-dark cycle (lights on at 06:00 AM). All animal procedures were conducted in accordance with the National Institutes of Health (NIH) Guide for the Care and Use of Laboratory Animals and approved by the Institutional Animal Care and Use Committee of Augusta University.

Behavioral tests

Mice of different ages were used for behavioral testing. Before the experiments, animals were transferred to a testing room and habituated to the room conditions for 3–4 h. All behavioral procedures were conducted during the late light cycle. The apparatus was cleaned with 20% ethanol and dried after each trial to remove olfactory cues. Behavioral responses were analyzed by experimenters who were blind to genotypes and treatment.

Y-maze spontaneous alternation test. Short-term spatial working memory was assessed using a Y-maze consisting of three arms (length \times width \times height: $30\times6\times15$ cm) positioned at 120° to each other (Panlab Harvard Apparatus, MA, USA). Each mouse was placed at the end of one arm facing the center of the maze and allowed to freely explore all three arms of the maze for 10 min. The sequence and frequency of arm entries were recorded to evaluate spontaneous alternations. An entry was defined as all four limbs being inside an arm. Spontaneous alternation reflects the natural tendency of mice to explore previously unvisited arms of the maze, driven by their innate curiosity and a preference for novelty. Spontaneous alternation [%] was calculated as (number of consecutive entries into three different arms) / (total number of arm entries - 2) \times 100% [31]. Total numbers of arm entries were used as a measure of activity and locomotion during the testing session.

Novel object recognition (NOR) test. The NOR test has been widely used to assess object recognition memory, which is based upon rodent's innate tendency to explore novel objects over familiar ones [32-34]. This test was performed in a white acrylic apparatus consisting of a 40 × 40 cm openfield arena with 40 cm high walls $(40 \times 40 \times 40 \text{ cm})$. The test consisted of four sequential sessions: one habituation session, one training session and two testing sessions. The NOR task can be used to examine short-term memory or probe long-term memory by manipulating the retention interval, i.e. the amount of time animals retain memory of the objects presented during the training session. On the first day of the test, each mouse was placed individually in the empty open arena and allowed to explore for 5 min to habituate to the testing environment (habituation session). On the second day, two identical objects were placed in the arena, located close to two adjacent corners. The mouse was released at the center of the wall opposite the objects, facing away from them, and allowed to freely explore them for 5 min (training session). After a 2-h retention interval, a novel object (N1) was introduced to the arena and the mouse was returned to the arena and allowed to explore the familiar and novel objects for 5 min (testing session 1). The location of novel versus familiar object was counterbalanced. Testing session 2 was performed after a 24-h retention interval in the same arena with a second novel object (N2). The mouse was allowed to explore familiar and novel (N2) objects for 5 min. The time spent exploring the novel object versus the familiar one was recorded. The preference for the novel object reflects the ability to discriminate between a familiar object and a novel object, used as an index of short-term object recognition memory after a 2-h retention interval or long-term recognition memory after a 24-h retention interval. The discrimination index was calculated as: (Time exploring novel object -Time spent exploring familiar object) / Total object exploration time. This index provides a normalized measure of preference for the novel object relative to total exploration time.

Three-chamber social test. This test has been widely used for assessing sociability and social recognition memory in mice, based on their natural preference for social interaction and their ability to discriminate between familiar and novel social targets. The testing apparatus was a rectangular box $(60 \times 40 \times 20 \text{ cm})$, which was divided into three chambers of equal size that were interconnected by small opening doors (3 × 4 cm). The testing procedure consisted of four sequential sessions: (1) 5-min habituation: mice were allowed to acclimate to the central chamber with both connecting doors closed. (2) 10-min exploration: mice were allowed to freely explore all three chambers, with each side chamber containing a wire cup. (3) 10-min social interaction: in this session, mice explored the three chambers again. One side chamber contained a wire cup with an age- and sex-matched novel mouse (S1) and the other side chamber contained a wire cup with a novel object (NS). (4) 10-min social recognition: during this phase, mice explored the three chambers with one side chamber now containing the familiar mouse from session 3 (S1), and the other side chamber held a wire cup with a novel mouse (S2). To minimize stress, novel mice were pre-habituated to the wire cups and chambers for 15 min per day for three days before being used for the test. The locations of the wire cages containing the novel object and novel mice (S1) were randomized and counterbalanced across the test animals. Exploratory behavior was monitored, and the time spent exploring in each chamber was analyzed using EthoVision XT (Leesburg, VA). For sociability analysis, the social preference index was calculated as (Time spent in the chamber with S1 - Time spent in the chamber with NS) / (Time spent in the chamber with S1 + Time spent in the chamber with NS). To assess social recognition memory, the social recognition index was calculated as (Time

spent in the chamber with S2 - Time spent in the chamber with S1) / (Time spent in the chamber with S2 + Time spent in the chamber with S1).

Metabolic assessments

Metabolic assessments were conducted using the Home Cage Comprehensive Lab Animal Monitoring System (HC-CLAMS) from Columbus Instruments (Columbus, OH, USA). This system enables a thorough examination of metabolism, energy expenditure, feeding and drinking patterns, and activity levels in mice. The system was housed in a controlled environment with a constant temperature, a regular light-dark cycle, and acoustic isolation. Mice were habituated to the HC-CLAMS for 12 h before data collection. Food intake, water intake, O_2 consumption (VCO2), and horizontal and vertical activity were monitored through the light and dark cycle. Respiratory exchange ratio (RER, VCO2/VO2), heat production [3.815 + 1.232RER) \times VO2] and locomotor activity were analyzed for a 24 h period.

Chronic social isolation-unpredictable stress

Mice were individually housed and exposed to various stressors at varying times of the day in an unpredictable manner for 10 consecutive days. Stressors included 2-h restraint, 15-min tail pinch, 24-h constant light, 24-h wet bedding with a 45° cage tilt, 10-min scrambled and inescapable foot shocks, 30-min elevated platform exposure [27–30]. All stress procedures were conducted in a procedure room. In contrast, control mice were group housed and received brief daily handling in the housing room. Behavioral tests were performed 24 h following the last stress session. Mice were perfused after behavioral testing to collect brain tissue for immunohistochemical staining of $\Delta\beta$.

Immunohistochemical staining and quantification of $A\beta$ plaques on brain sections

Mice were transcardially perfused under anesthesia through the ascending aorta using 0.1 M phosphate buffer (PB) followed by 4% paraformaldehyde (PFA) in PB. After perfusion, the brains were removed and post-fixed overnight in 4% PFA and then transferred to 30% sucrose in PBS for cryoprotection. The brains were cut into 40-µm coronal sections and stored in a cryoprotectant (30% sucrose, 30% ethylene glycol, 1% polyvinyl pyrrolidone, 0.05 M sodium phosphate buffer) until processing for immunohistochemistry. The free-floating sections were first rinsed with 0.05 M Tris-buffered saline (TBS) and then incubated in 0.5% Triton-X 100 in TBS for 60 min, followed by incubation with a blocking buffer (10% donkey serum and 0.5% Triton-X 100 in TBS) for 1.5 h at room temperature. Next, the brain sections were incubated with an AB antibody (clone 6E10, Novus Biologicals, #NBP2-62566, 1:750) overnight at 4°C. The brain sections were then rinsed in TBS buffer four times (10 min each) and incubated with a donkey anti-rabbit IgG (H + L) secondary antibody conjugated to Alexa Fluor 488 (1:500, Thermo Fisher Scientific, Waltham, MA) at room temperature for 2 h. The sections were washed with TBS four times (10 min each) and then mounted on slides with an aqueous anti-fade mounting medium. KEYENCE All-in-One Fluorescence Microscope BZ-X800 (Keyence Corporation of America, Itasca, IL) and Nikon A1R MP + Multiphoton Confocal Microscope were used to visualize immunostaining and capture images. Quantitative analysis of Aß plaque load in the entorhinal cortex, hippocampus and prefrontal cortex was conducted using ImageJ/ Fiji software [35]. Within the selected brain regions of each hemisphere, a consistent intensity threshold was set to identify specific staining. The AB plaque load was defined as the percentage of the area covered by $A\beta$ plaques (% area). Female 5xFAD mice displayed a more pronounced plaque pathology compared to age-matched male mice [7, 36]. For data combining male and female mice, Aß plaque load was normalized to the control mice of each respective sex and then these normalized measurements were pooled together for statistical analysis.

Whole-brain clearing, staining for $A\beta$ deposition and 3-D imaging

Tissue clearing and staining. Mice were transcardially perfused using PB and PFA as described above. Brains were processed for solvent-based clearing and immunolabeling according to the iDISCO protocol, as described previously [37–39]. Initial dehydration through increasing concentrations of methanol (MeOH) was carried out in 3-h steps before overnight delipidation in dichloromethane. The brains were subsequently bleached in $\rm H_2O_2$ (5% v/v in MeOH) before rehydration through decreasing concentrations of MeOH according to published methodology [38]. After

rehydration, the brains were incubated overnight in a blocking solution containing 0.2% Triton X-100, 10% DMSO, and 6% donkey serum in PBS at 37 °C. Samples were then washed twice (3 h each) in PBS containing 0.2% Tween-20 with 10 μ g/ml heparin (PTwH) before incubation with an Alexa Fluor 647-conjugated rabbit monoclonal anti-human A β antibody (Cell Signaling, Cat# 42284S, 1:250 in blocking solution) for 12–14 days with shaking. After incubation, samples were washed twice (3 h each), then overnight in PTwH. This sequence was repeated the following day before final dehydration through MeOH, delipidation in dichloromethane, and refractive index matching in dibenzyl ether, as previously reported [38].

Whole-brain 3D imaging and image processing. Cleared brains were stored in dibenzyl ether until imaging on a LaVision UltraMicroscope II light sheet microscope (Miltenyi Biotec) equipped with a LVMI-Fluor 4×/0.3 WD6 objective lens and an Andor sCMOS camera. Samples were placed into the sample holder and imaged along the sagittal plane in the chamber filled with dibenzyl ether. Images were acquired at 4×magnification with 0.6 × zoom (resolution of 0.37 pixels/μm) in a z-stack at 10 μm intervals. Aβ detection was captured with an excitation wavelength of 639 nm and an emission wavelength of 680 nm (30 nm bandpass) and autofluorescence was captured at a wavelength of 488 nm with an emission of 525 nm (50 nm bandpass). Tiles were stitched using Terastitcher [40] and stitched images were pre-processed using a scale-invariant block matching filter (XY radius = $7.4 \mu m$, sigma = 3) in ImageJ/Fiji [41]. After processing, autofluorescence images were subtracted from images of AB and suprathreshold particles were masked based on size and circularity criteria $(>150 \, \mu m^2$, circularity > 0.5) with ImageJ/Fiji. The masked images were imported into NeuroInfo software (MBF Bioscience) for alignment and registration to the Allen Brain Atlas Common Coordinate Framework. Volumetric measurements and plaque quantification were performed within each annotated structure, allowing for detailed regional comparisons of Aβ pathology across ages.

Statistical analysis

All results are presented as mean ± s.e.m. (standard error of the mean). Normality and equal variance assumptions were assessed by using the Shapiro-Wilk test and F test, respectively. For comparisons between two groups, two-tailed unpaired t-tests were employed for normally distributed data with equal variance. In the case of normally distributed data with unequal variance, unpaired t-tests with Welch's correction were utilized, while Mann-Whitney nonparametric tests were applied to analyze nonnormally distributed data. Within-group comparisons of exploration time on familiar and novel objects in the NOR test and time spent in chambers with different stimuli in the three-chamber social test were conducted using paired t-tests for normally distributed data and Wilcoxon matchedpairs signed rank tests for non-normally distributed data. To assess the stress and genotype effects on behavioral performance, two-way ANOVAs followed by Bonferroni post hoc tests were used. In CLAMS studies, different parameters across the light-dark cycle were analyzed using twoway repeated-measures ANOVAs followed by Bonferroni post hoc tests. In all statistical analyses, a P value of < 0.05 was considered statistically significant.

RESULTS

Characterization of age-dependent cognitive phenotypes in 5xFAD mice

In this study, we used hemizygous 5xFAD mice on a congenic C57BL/6 J background for all experiments, generated by breeding hemizygous male 5xFAD mice (C57BL/6 J) with wild-type female C57BL/6 J mice. Multiple behavioral tests targeting distinct cognitive domains, including the Y-maze spontaneous alternation, novel object recognition and three-chamber social tests, were employed to characterize the cognitive phenotype of 5xFAD mice at different ages. These tests were selected because they assess cognitive functions without introducing external stressors or aversive stimuli that could potentially influence performance.

Spatial working memory deficits in 5xFAD mice. We first assessed short-term spatial working memory using the Y-maze spontaneous alternation test in mice at different ages. Spontaneous alternation in this test, which is driven by an innate curiosity to

explore previously unvisited areas, serves as a measure of spatial working memory. Typically, impairments in spatial working memory manifest as a reduced rate of spontaneous alternation in the Y-maze test. Importantly, this test does not necessitate any prior training and can be administered repeatedly, allowing for multiple assessments and longitudinal studies in mice to monitor cognitive changes over time. Male 5xFAD mice showed normal spontaneous alternation rates and comparable arm entries during the test at 3-6 months of age when compared with age- and sexmatched wild-type littermate control mice (Fig. 1A2; spontaneous alternation %: $t_{43} = 0.023$, P = 0.982; total arm entries: $t_{43} = 1.494$, P = 0.143). At 9-10 months of age, 5xFAD mice exhibited significantly lower percentage of spontaneous alternation (Fig. 1A3; $t_{23} = 2.496$, P = 0.020), indicating impaired spatial working memory. In addition, 5xFAD mice at 9-10 months of age showed an increase in total arm entries (unpaired t-test with Welch's correction, P = 0.007) compared with wild-type mice.

Short-term and long-term object recognition memory deficits in 5xFAD mice. Novel object recognition memory can be evaluated in both humans and rodents through analogous principles to assess the ability to recall and differentiate between familiar and novel objects [42]. Male 5xFAD mice and their wild-type littermate control mice, aged 8-9 months, were tested for short-term object recognition memory after a 2-h retention interval following the training phase (Fig. 1B). While wild-type mice at 8-9 months of age spent significantly more time exploring the novel object compared to the familiar object (Wilcoxon matched-pairs signed rank test, P = 0.002), 5xFAD mice at this age showed no preference for the novel object over the familiar object (paired t-test, $t_6 = 0.909$, P = 0.399) (Fig. 1B2). To rule out the confounding effects of overall exploration on the assessment of recognition memory, the difference in exploration time between the novel and familiar objects were normalized by the total investigation time of individual mice and expressed as a discrimination index. A significantly reduced discrimination index was observed in 5xFAD mice compared to wild-type controls ($t_{16} = 3.942$, P = 0.001), thus indicating impaired short-term object recognition memory. The long-term object recognition memory was evaluated by introducing another novel object after a 24-h retention interval following the training phase. As shown in Fig. 1B3, wild-type control mice invested a substantially greater amount of time in exploring the novel object (Wilcoxon matched-pairs signed rank test, P = 0.007), whereas 5xFAD mice failed to show preference for the novel object over the familiar object (paired t-test, $t_6 = 0.429$, P = 0.683) (Fig. 1B3), consistent with a significant reduction in the discrimination index in the 5xFAD mice ($t_{16} = 3.254$, P = 0.005). These findings indicate that 5xFAD mice at 8-9 months of age exhibit impaired short-term and long-term object recognition memory.

Social recognition memory in 5xFAD mice. The three-chamber social test is designed to assess an animal's preference for social interaction and its ability to recognize and distinguish other conspecifics. Both sociability and social recognition were evaluated in male 5xFAD and wild-type control mice at 4 and 8 months of age (Fig. 2A). Both 5xFAD mice and wild-type control mice showed an intact preference for social interaction at 4 months of age, as evidenced by spending more time exploring the chamber containing a novel mouse compared to the chamber containing an object (Fig. 2B; wild-type: paired t-test, $t_8 = 3.559$, P = 0.007; 5xFAD: paired t-test, $t_8 = 3.108$, P = 0.015). Normalizing the difference in time spent between the two chambers containing the novel mouse and the novel object by the total time spent in both chambers produced the social preference index. 5xFAD and wild-type mice exhibited comparable social preference indices ($t_{16} = 0.215$, P = 0.833), indicating normal sociability and a natural inclination of the 5xFAD mice to engage in social interactions at a young age. During the social recognition testing session, 4-month-old 5xFAD mice spent more time exploring and interacting with the unfamiliar mouse compared to the familiar one (Wilcoxon matched-pairs signed rank test, P = 0.020), similar to wild-type control mice (paired t-test, $t_8 = 2.749$, P = 0.025). Normalizing the difference in time spent between the two chambers containing the novel and familiar social stimuli by the total time spent in both chambers produced the social recognition index, which reflects the degree to which a mouse shows recognition and preference for an unfamiliar mouse over the previously encountered one. The social recognition index was comparable between wild-type and 5xFAD mice ($t_{16} = 0.456$, P = 0.654), suggesting that 5xFAD mice at 4 months of age retain the ability to recognize and respond to social novelty. By 8 months of age, 5xFAD mice continued to show a normal preference for a novel mouse over an object in the sociability test (Fig. 2C; wildtype: paired t-test, $t_6 = 4.946$, P = 0.003; 5xFAD: paired t-test, $t_5 = 2.603$, P = 0.048). When compared with wild-type mice, 5xFAD mice exhibited a similar preference index in the sociability test $(t_{11} = 0.564, P = 0.584)$. However, in the social recognition test, 8month-old 5xFAD mice failed to discriminate between the familiar and unfamiliar mouse (wild-type: paired t-test, $t_6 = 10.09$, P < 0.001; 5xFAD: paired t-test, $t_5 = 0.338$, P = 0.749). 5 × FAD mice at this age showed a significant reduction in the social recognition index compared with age-, sex-matched wild-type littermate controls (unpaired t test with Welch's correction, P = 0.049), indicating an impairment in social recognition memory.

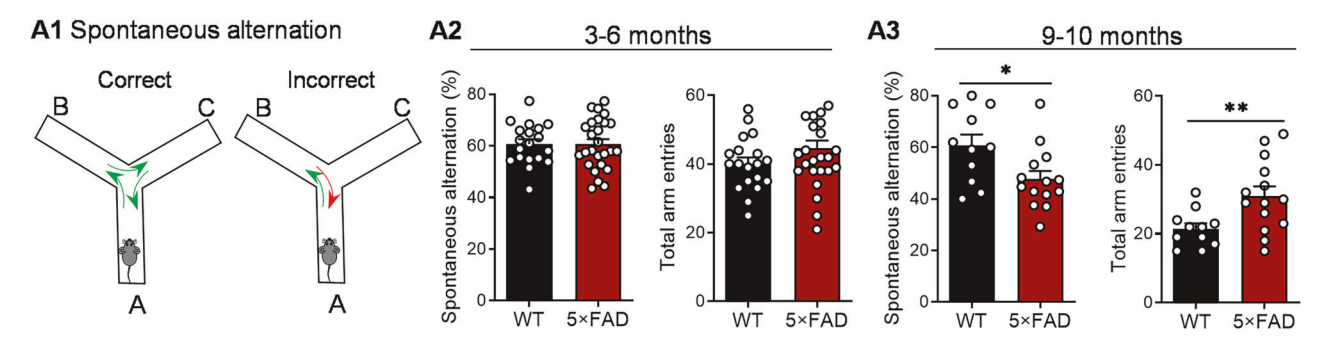
Whole-brain imaging of $A\beta$ deposition in 5xFAD mice at different ages

Given the age-dependent development of cognitive phenotypes in 5xFAD mice, we examined the progression of A β plaque deposition in the brains of male congenic C57BL/6 J 5xFAD mice across different ages. First, the distribution of A β plaques in coronal brain sections was assessed at 2, 4 and 8 months of age, focusing on the forebrain regions, particularly the cortex and hippocampus implicated in learning and memory. At 2 months of age, A β plaques were very sparse to undetectable in most forebrain regions, including the hippocampus and prefrontal cortex, except for the subiculum, where plaques were more evident. By 4 months of age, A β plaques became detectable in many brain regions, including the cortex, hippocampus, and entorhinal cortex. A β deposition continued to increase, becoming more widespread and prominent by 8 months of age (Fig. 3A).

We then proceeded to assess and compare the threedimensional (3D) spatial distribution of AB at 4 months and 8 months using light sheet whole-brain mapping technology. This spatial information is important for identifying regional patterns in the entire brain and understanding the development of AB deposition across different brain regions and ages. The iDISCO method, a whole-mount immunolabeling and brain clearing technique, allows for volumetric imaging of AB plaques throughout the intact brain (Fig. 3B). NeuroInfo was utilized to precisely map Aβ signals onto the annotated mouse brain atlas (Fig. 3C, D), and AB plaques were quantified in eight major brain regions. As shown in Fig. 3E, the number of Aβ plaques was higher in the isocortex $(t_4 = 3.605, P = 0.023)$, hippocampus $(t_4 = 3.438,$ P = 0.026), entorhinal cortex ($t_4 = 4.279$, P = 0.013), hypothalamus $(t_4 = 4.733, P = 0.009)$, pons $(t_4 = 3.943, P = 0.017)$, and medulla $(t_4 = 4.389, P = 0.012)$ of 5xFAD mice at 8 months of age compared to 4 months, whereas no significant increase was observed in the thalamus ($t_4 = 1.282$, P = 0.269) or midbrain $(t_4 = 1.978, P = 0.119)$. Furthermore, volumetric measurements and plague quantification were performed within each annotated structure, allowing for subregional comparisons of AB pathology across two different ages. As shown in Fig. 3F, compared to 4 months of age, 5xFAD mice at 8 months of age showed significantly more Aβ plaques in the anterior cingulate area (ACA, $t_4 = 3.315$, P = 0.030), prelimbic area (PL, $t_4 = 3.851$, P = 0.018),

4724

A Y-maze test



B Novel object recognition test (8-9 months)

B1 Experimental procedure

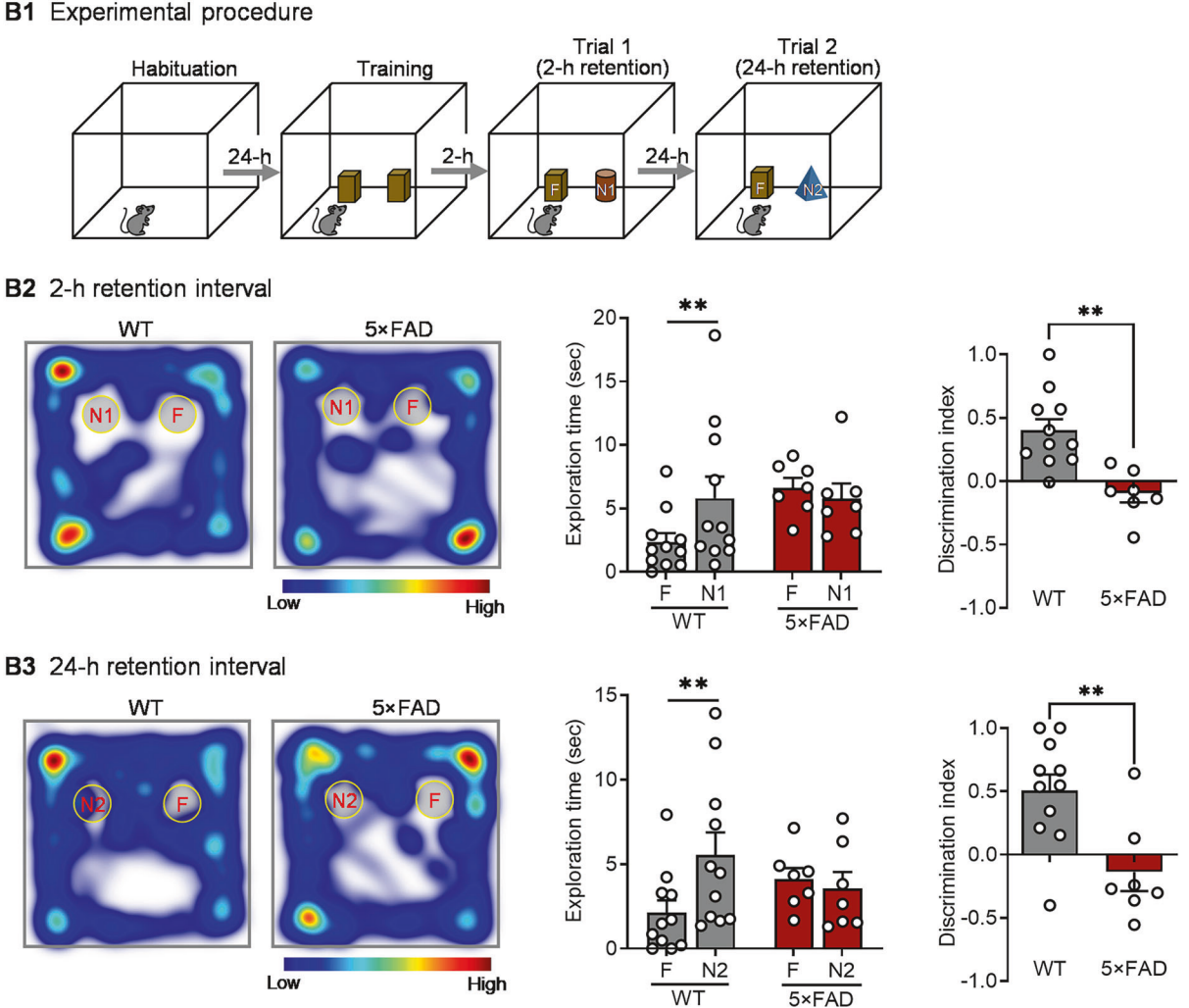


Fig. 1 Age-dependent impairments in spatial working memory and object recognition memory in 5xFAD mice. A Y-maze spontaneous alternation test. (A1) Schematic of the Y-maze test. (A2-A3) Spontaneous alternation rate (left) and total arm entries (right) of male 5xFAD mice and WT littermate control mice tested at 3–6-months old (A2) and 9–10-months old (A3). A2: WT, n = 19; 5xFAD, n = 26. A3: WT, n = 11; 5xFAD, n = 14. *P < 0.05, *P < 0.01 compared with WT mice. **B** Novel object recognition (NOR) test. (**B1**) Schematic of the experimental procedure of the NOR test. (B2) Trial 1 with a 2-h retention interval. Left, representative images of heat maps depicting the time spent by the mice in the test arena. Middle, exploration time between familiar (F) and novel object 1 (N1). Right, discrimination index. (B3) Trial 2 with a 24h retention interval. Left, representative images of heat maps depicting the time spent by the mice in the test arena. Middle, exploration time between familiar (F) and novel object 2 (N2). Right, discrimination index. n = 7-11 male mice per group. For exploration time, **P < 0.01, paired t-test compared between familiar and novel object. For discrimination index, **P < 0.01 compared with WT mice.

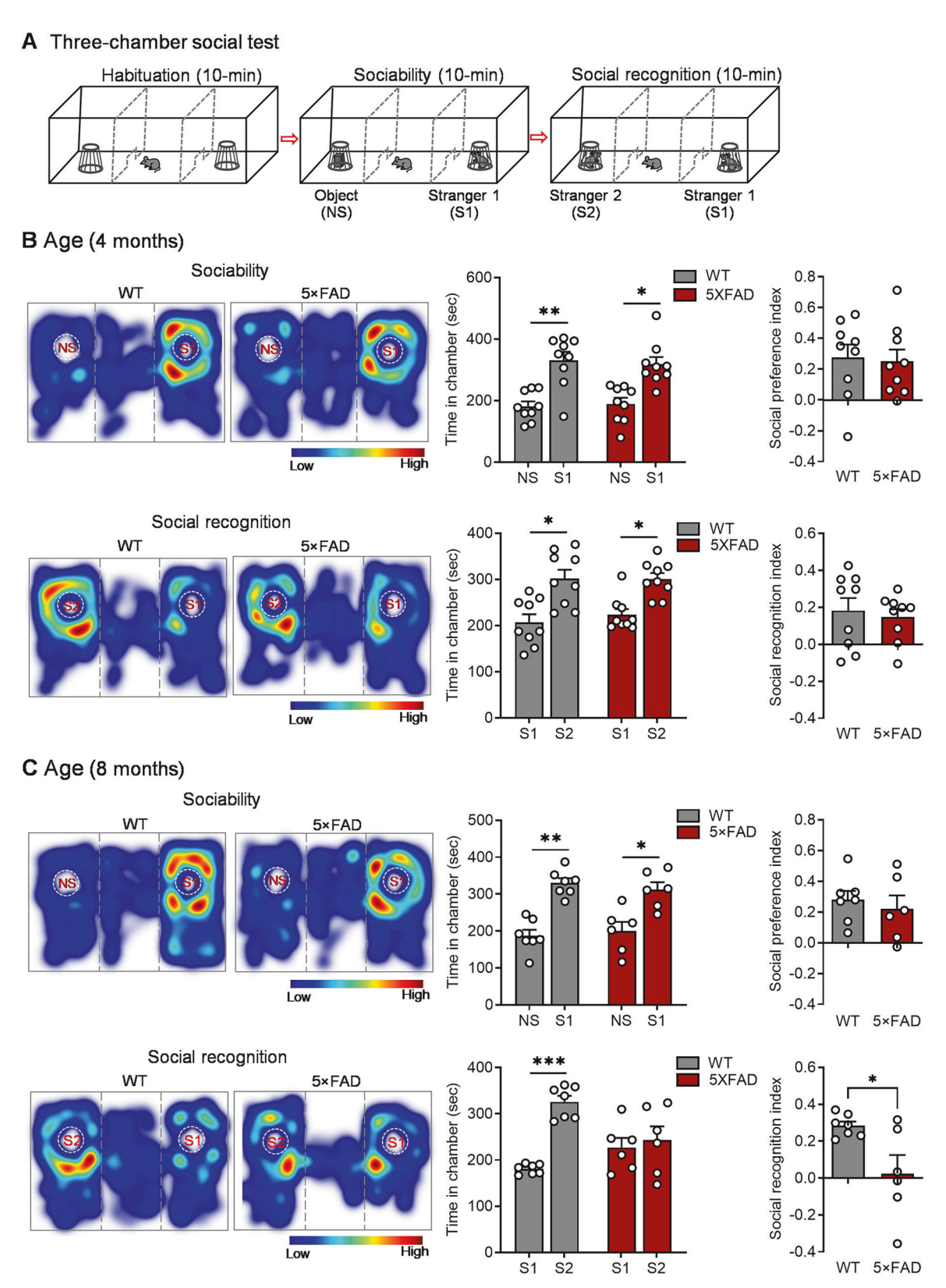
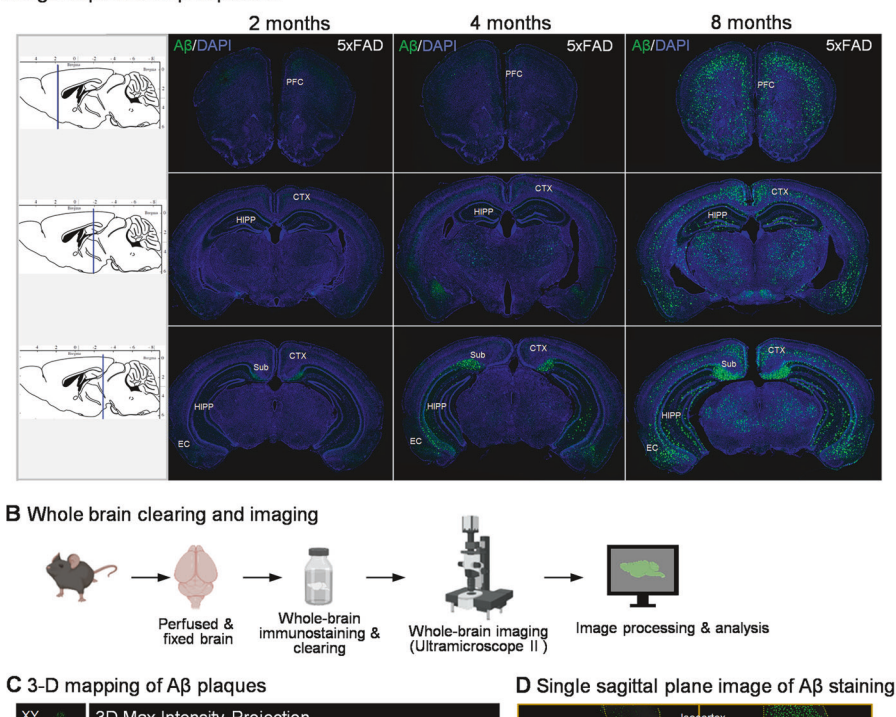
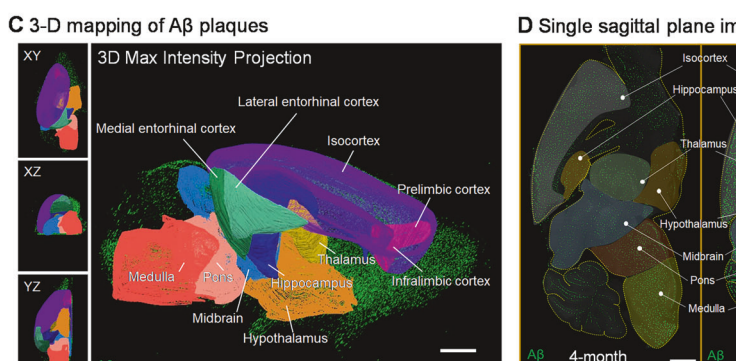
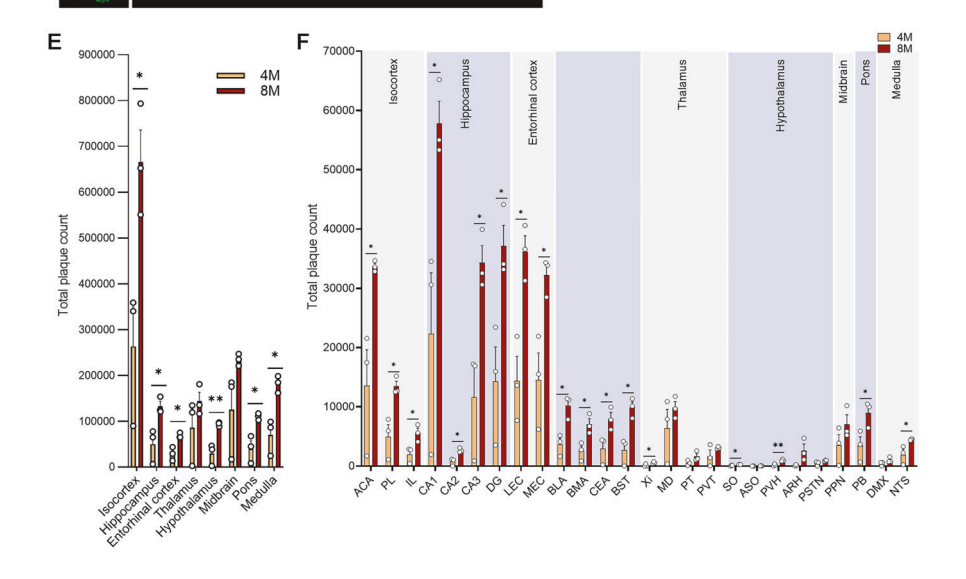


Fig. 2 Age-dependent impairment of social recognition memory in 5xFAD mice. A Schematic of the 3-chamber sociability and social recognition test. B Three-chamber social test on 4-month-old mice. n = 9 male mice per group. C Three-chamber social test on 8-month-old mice. n = 6-7 male mice per group. B, C Upper panel: Sociability test. Upper left, representative images of heat maps depicting the time spent in each chamber. Upper middle, time spent in chamber with novel object (NS) and stranger mouse 1 (S1). Upper right, social preference index. Lower panel: Social recognition test. Lower left, representative images of heat maps depicting the time spent in each chamber. Lower middle, time spent in chamber with stranger mouse 1 (S1) and stranger mouse 2 (S2). Lower right, social recognition index. For time in chamber, *P < 0.05, *P <

A Age-dependent Aβ deposition







infralimbic area (IL, $t_4 = 3.099$, P = 0.036), hippocampal CA1 ($t_4 = 3.252$, P = 0.031), CA2 ($t_4 = 4.599$, P = 0.010), CA3 ($t_4 = 3.724$, P = 0.020), dentate gyrus (DG, $t_4 = 3.368$, P = 0.028), lateral entorhinal cortex (LEC, $t_4 = 4.423$, P = 0.012), medial entorhinal cortex (MEC, $t_4 = 3.595$, P = 0.023), basolateral

amygdalar nucleus (BLA, t_4 = 4.177, P = 0.014), basomedial amygdalar nucleus (BMA, t_4 = 3.493, P = 0.025), central amygdalar nucleus (CEA, t_4 = 2.860, P = 0.046), bed nuclei of the stria terminalis (BST, t_4 = 4.377, P = 0.012), xiphoid thalamic nucleus (Xi, t_4 = 2.787, P = 0.049), supraoptic nucleus(SO, t_4 = 3.418,

Fig. 3 Whole-brain analysis of Aβ plaque accumulation in 5xFAD mice. A Staining of Aβ plaques on coronal brain sections at the indicated ages. The drawings of the sagittal planes were adapted from the Atlas of Paxinos and Franklin [91] with blue lines indicating the focal plane of coronal sections. PFC prefrontal cortex, CTX cortex, HIPP hippocampus, EC entorhinal cortex, Sub subiculum. B Schematic illustration of the iDISCO method for visualizing the whole-brain distribution of Aβ plaque accumulation. Illustrations were created with BioRender.com. C Each image stack was registered to the 3-D Allen Mouse Brain Atlas. D A single sagittal plane image showing the deposition of Aβ plaques in the brain at 4 and 8 months of age. E Quantification of Aβ plaques in eight major brain structures. The hippocampus here refers to the dentate gyrus and hippocampus proper (CA1-3), not including the subicular cortex. F Quantification of Aβ plaques for subregional comparisons between two age groups. Scale bar = 1000 μm. n = 3 male mice per group. * $^*P < 0.05$, * $^*P < 0.01$ at 8-month-old compared with 4-month-old. ACA anterior cingulate area, PL prelimbic cortex, IL infralimbic cortex, DG dentate gyrus, LEC lateral entorhinal cortex, MEC medial entorhinal cortex, BLA basolateral amygdalar nucleus, BMA basomedial amygdalar nucleus, CEA central amygdalar nucleus, BST bed nuclei of the stria terminalis, Xi xiphoid thalamic nucleus, MD mediodorsal nucleus of thalamus, PT parataenial nucleus, PVT paraventricular nucleus of the thalamus, SO supraoptic nucleus, ASO accessory supraoptic group, PVH paraventricular hypothalamic nucleus, ARH arcuate hypothalamic nucleus, PSTN parasubthalamic nucleus of the vagus nerve, NTS nucleus of the solitary tract.

P=0.027), paraventricular hypothalamic nucleus (PVH, $t_4=5.350$, P=0.006), parabrachial nucleus (PB, $t_4=2.810$, P=0.048) and nucleus of the solitary tract (NTS, $t_4=2.828$, P=0.047). The other assessed brain regions did not show a significant age-related increase in Aβ plaque count, including the mediodorsal nucleus of the thalamus (MD, $t_4=1.039$, P=0.358), parataenial nucleus (PT, $t_4=1.989$, P=0.118), paraventricular nucleus of the thalamus (PVT, $t_4=1.337$, P=0.252), accessory supraoptic group (ASO, $t_4=1.205$, P=0.295), arcuate hypothalamic nucleus (ARH, $t_4=2.354$, P=0.078), parasubthalamic nucleus (PSTN, $t_4=2.128$, P=0.101), pedunculopontine nucleus (PPN, $t_4=1.495$, P=0.209) and dorsal motor nucleus of the vagus nerve (DMX, $t_4=1.853$, P=0.137).

Characterization of age-dependent metabolic changes in 5xFAD mice

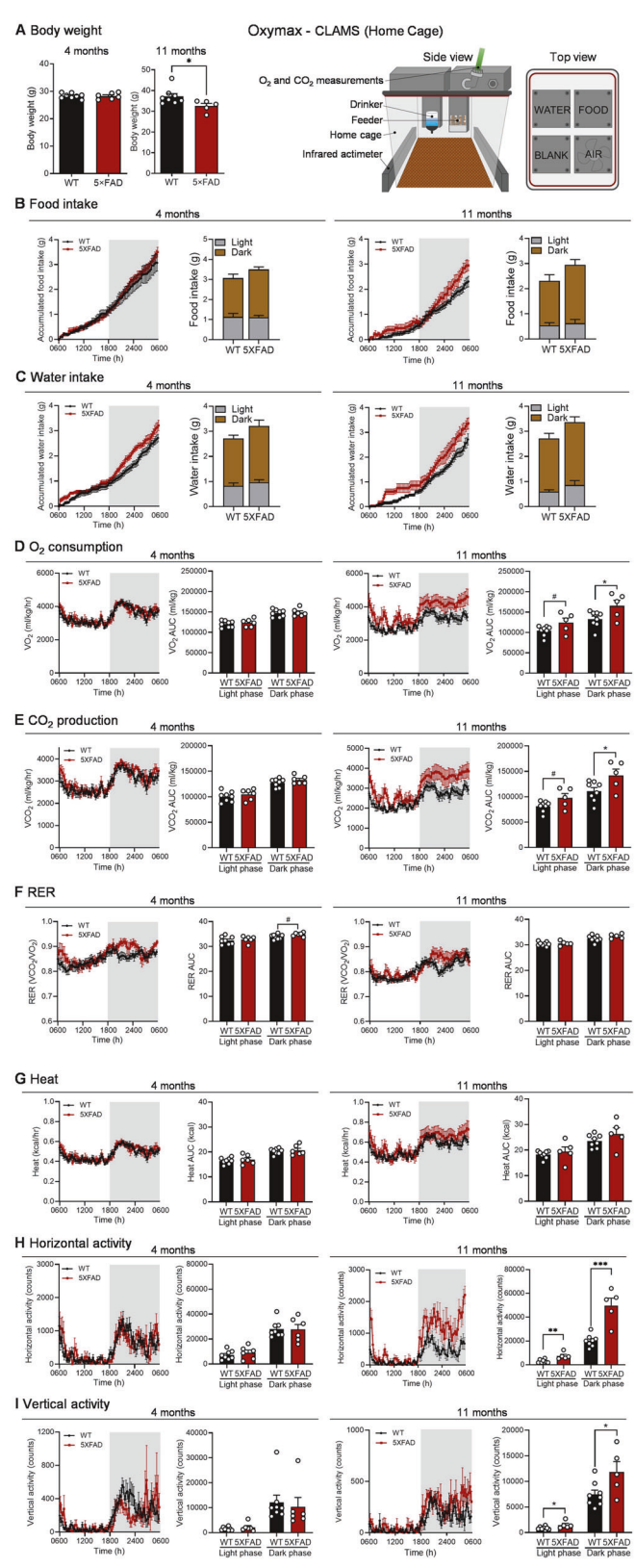
5xFAD mice at 4 months of age exhibited a body weight comparable to that of wild-type mice (Fig. 4A, $t_{12} = 0.113$, P = 0.912). Feeding, drinking, energy expenditure and activity were assessed by using HC-CLAMS with their home cages, which allowed for the monitoring of metabolic parameters and locomotor behavior of mice in their familiar environment. This approach is less stressful for mice and facilitates their acclimation to the monitoring system (Fig. 4A). The cumulative food intake over a 24-h period, as measured by CLAMS, was similar in 5xFAD mice and wild-type mice, with no significant difference observed (Fig. 4B; food intake curve: time, $F_{(79,790)} = 182.6$, P < 0.001, genotype, $F_{(1.10)} = 0.166$, P = 0.692time × genotype, $F_{(79,790)} = 0.726$, P = 0.963). Furthermore, total food intake showed no genotype difference in either the light phase or in the dark phase when considered separately (light phase: $t_{10} = 0.143$, P = 0.890; dark phase: Mann Whitney test, P = 0.132). Drinking behavior was also monitored by CLAMS. 5xFAD mice showed increased water intake over a 24-h period compared with wildtype mice (Fig. 4C; ANOVA: time, $F_{(79,948)} = 247.5$, P < 0.001, $F_{(1,12)} = 5.612,$ P = 0.036, time × genotype, $F_{(79.948)} = 2.542$, P < 0.001), but when total water intake was divided into the light and dark phases, no significant genotype difference was observed (light phase: $t_{12} = 0.926$, P = 0.373; dark phase: $t_{12} = 1.382$, P = 0.192).

Basal energy expenditure, as measured by oxygen consumption (VO₂) and carbon dioxide production (VCO₂), showed no significant difference between 5xFAD mice and wild-type mice at 4 months of age (Fig. 4D; VO₂: time, $F_{(79,948)} = 11.42$, P < 0.001, genotype, $F_{(1,12)} = 0.336$, P = 0.573, time × genotype, $F_{(79,948)} = 0.878$, P = 0.765. Figure 4E; VCO₂: time, $F_{(79,948)} = 12.75$, P < 0.001, genotype, $F_{(1,12)} = 1.105$, P = 0.314, time × genotype, $F_{(79,948)} = 0.924$, P = 0.664). Analysis of the area under the curve (AUC), a sum of the cumulative values of VO₂ and VCO₂, for the light and dark cycles separately also showed no genotype differences (VO₂: light phase: $t_{12} = 0.752$, P = 0.467; dark phase: $t_{12} = 0.387$, P = 0.706. VCO₂: light phase: $t_{12} = 0.804$, P = 0.437;

dark phase: $t_{12} = 1.265$, P = 0.230). Furthermore, the respiratory exchange ratio (RER) was calculated from the ratio of VCO₂ produced to VO₂ consumed as a measure of the relative contribution of carbohydrates and lipids to overall energy expenditure. Results in 5xFAD mice were similar compared with wild-type mice (Fig. 4F; RER curve: time, $F_{(79.948)} = 7.878$, P < 0.001, P = 0.263, $F_{(1,12)} = 1.379,$ time × genotype, genotype, $F_{(79,948)} = 1.779$, P < 0.001). Although not statistically significant, the sum of the RER (AUC) during the dark cycle tended to be increased in 5xFAD mice compared to the wild-type control group (RER-AUC: light phase: $t_{12} = 0.553$, P = 0.591; dark phase: $t_{12} = 1.984$, P = 0.071). This suggests that there may be a trend towards a higher reliance on carbohydrates as a fuel source in 5xFAD mice.

In addition, 5xFAD and wild-type mice at 4 months of age had similar heat production over a 24-h period, as determined by the sum of heat production (AUC) and analyzed separately for the light and dark cycles (Fig. 4G; Heat curve: time, $F_{(79.948)} = 11.89$, P < 0.001, genotype, $F_{(1,12)} = 0.318$, P = 0.583, time × genotype, $F_{(79.948)} = 0.884$, P = 0.753. Heat-AUC: light phase: $t_{12} = 0.643$, P = 0.533; dark phase: $t_{12} = 0.468$, P = 0.648). Moreover, at this relatively young age, 5xFAD mice showed no significant differences in horizontal activity (Fig. 4H; Horizontal activity: time, $F_{(79,948)} = 9.277$, P < 0.001, genotype, $F_{(1,12)} = 0.055$, P = 0.818, time × genotype, $F_{(79,948)} = 1.320$, P = 0.037. Horizontal activity-AUC: light phase, $t_{12} = 0.830$, P = 0.423; dark phase, $t_{12} = 0.053$, P = 0.959) or vertical activity (Fig. 4I; Vertical activity: time, $F_{(79.948)} = 6.595$, P < 0.001, genotype, $F_{(1.12)} = 0.042$, P = 0.842, time × genotype, $F_{(79,948)} = \overline{1.668}$, P = 0.0004. Vertical activity-AUC: light phase, Mann Whitney test, P = 0.755; dark phase, Mann Whitney test, P = 0.181) compared to wild-type mice.

However, by the age of 11 months, 5xFAD mice displayed changes in body weight and metabolic dynamics. First, 11-monthold 5xFAD mice showed a significant decrease in body weight compared to age-matched wild-type mice (Fig. 4A, Mann Whitney test, P = 0.019). The decreased body weight could result from decreased energy intake and/or increased energy expenditure. Unexpectedly, total food intake and water intake over a 24-h period tended to be increased in 5xFAD mice compared to wildtype mice (Fig. 4B; cumulative food intake: time, $F_{(79,790)} = 133.8$, P < 0.001, genotype, $F_{(1,10)} = 3.136$, P = 0.107, time × genotype, $F_{(79,790)} = 2.068$, P < 0.001; total food intake: light phase, $t_{10} = 0.472$, P = 0.647; dark phase, $t_{10} = 1.601$, P = 0.141) (Fig. 4C; cumulative water intake: time, $F_{(79,869)} = 155.9$, P < 0.001, genotype, $F_{(1,11)} = 9.123$, P = 0.012, time × genotype, $F_{(79.869)} = 2.320$, P < 0.001; total water intake: light phase: $t_{11} = 1.553$, P = 0.149; dark phase: Mann Whitney test, P = 0.222). Analysis of energy expenditure over a 24-h period revealed that 5xFAD mice consumed more O₂ and produced more CO₂ compared to wildtype control mice (Fig. 4D, E; VO₂ curve: time, $F_{(79,869)} = 16.45$, P < 0.001, genotype, $F_{(1,11)} = 4.939$, P = 0.048, time × genotype, $F_{(79.869)} = 1.630$, P < 0.001; VCO_2 curve: time, $F_{(79.869)} = 21.47$,



P < 0.001, genotype, $F_{(1,11)}$ = 5.063, P = 0.046, time × genotype, $F_{(79,869)}$ = 1.906, P < 0.001). Further analysis of the light cycle and dark cycle data indicated that the increases in O_2 consumption and CO_2 production were primarily observed during the dark cycle (VO_2 -light phase: t_{11} = 1.998, P = 0.071; VO_2 - dark phase: t_{11} = 2.319, P = 0.041; VCO_2 - light phase: t_{11} = 1.983, P = 0.073;

Fig. 4 Metabolic characterization of 4-month and 11-month-old 5xFAD mice. A Left, body weight. Right, automated home-cage CLAMS monitoring system. **B** Accumulated food intake and total food intake during light and dark phase. **C** Accumulated water intake and total water intake during light and dark phase. **D–H** Realtime monitoring curve and the area under curve (AUC) quantification of **D** O₂ consumption, **E** CO₂ production, **F** respiratory exchange ratio (RER), **G** heat production, **H** horizontal activity, and **I** vertical activity in light and dark cycle. n=5-8 male mice per group. *P<0.05, **P<0.01, ***P<0.01, ***P<0.001, **P<0.001, **P<0.001, **P<0.001, **P<0.001, ***P<0.001, **P<0.001, *

 VCO_2 - dark phase: $t_{11} = 2.343$, P = 0.039). This suggests that 5xFAD mice exhibited an increase in metabolic activity and energy utilization specifically during the period corresponding to the dark cycle. In contrast, the RER and heat production within a period of 24 h were comparable between 5xFAD mice and wild-type mice (Fig. 4F, G; RER curve: time, $F_{(79.869)} = 11.34$, P < 0.001, genotype, $F_{(1.11)} = 1.387$, P = 0.264, time × genotype, $F_{(79,869)} = 1.489$, P = 0.005; Heat curve: time, $F_{(79,869)} = 16.96$, P < 0.001, genotype, $F_{(1,11)} = 1.119$, P = 0.313, time × genotype, $F_{(79,869)} = 1.346$, P = 0.028;). Further analysis of data from the light and dark cycles showed no genotype differences (RER - light phase: $t_{11} = 0.454$, P = 0.659; RER - dark phase: $t_{11} = 1.421$, P = 0.183; heat - light phase: $t_{11} = 0.710$, P = 0.493; heat - dark phase: $t_{11} = 1.256$, P = 0.235). Overall, the RER data suggests that there were no significant differences in the balance between carbohydrate and lipid oxidation during energy expenditure in wild-type versus 5xFAD mice. In contrast, 5xFAD mice exhibited higher levels of both horizontal and vertical activity compared to the wild-type mice in both the light and dark cycles (Fig. 4H, I; horizontal activity curve: time, $F_{(79,869)} = 14.71$, P < 0.001, genotype, $F_{(1,11)} = 33.92$, P < 0.001, time × genotype, $F_{(79,869)} = 3.628$, P < 0.001; horizontal activity- light phase: Mann Whitney test, P = 0.003; horizontal activity - dark phase: $t_{11} = 5.560$, P < 0.001; vertical activity curve: time, $F_{(79.869)} = 8.590$, P < 0.001, genotype, $F_{(1.11)} = 7.691$, P = 0.018, time × genotype, $F_{(79,869)} = 1.275$, P = 0.060; vertical activity - light phase: $t_{11} = 2.202$, P = 0.049; vertical activity - dark phase: $t_{11} = 2.358$, P = 0.038). These results indicate agedependent increases in activity and energy expenditure in 5xFAD mice.

Onset of cognitive deficits in young 5xFAD mice following chronic social isolation-unpredictable stress

Social isolation and unpredictable stress have been used to study the impact of chronic stress on a variety of behaviors [27–30]. In our initial investigation, we assessed whether this stress paradigm could induce a persistent activation of the HPA axis in young wildtype (2-3-month-old) mice. After 10 days of social isolation and unpredictable stress, mice exhibited an increase in baseline corticosterone levels, as measured 24 h after the last stress session (control: $158.7 \pm 12.19 \text{ ng/ml}$; chronic stress: $335.2 \pm 56.27 \text{ ng/ml}$; unpaired t test with Welch's correction, P = 0.049), indicating hyperactivity of the HPA axis. To investigate whether this stress paradigm accelerates the expression of cognitive and neuropathological phenotypes of 5xFAD mice, we subjected young 5xFAD mice and wild-type littermate controls of both sexes (3-4 months old) to 10 days of social isolation and unpredictable stress (as shown in Fig. 5A). We measured body weight both before and after chronic stress exposure. First, data from male and female wild-type and 5xFAD mice were combined for statistical analysis. We observed a significant main effect of stress and a significant interaction effect between genotype and stress (Fig. 5B. Male + female: stress, $F_{(1,65)} = 136.9$, P < 0.001; genotype, P = 0.865; stress × genotype interaction, $F_{(1,65)} = 0.029,$ $F_{(1.65)} = 4.915$, P = 0.030). Then, male and female groups were analyzed separately to detect potential sex-specific effects of stress and genotype. We found that chronic stress decreased body

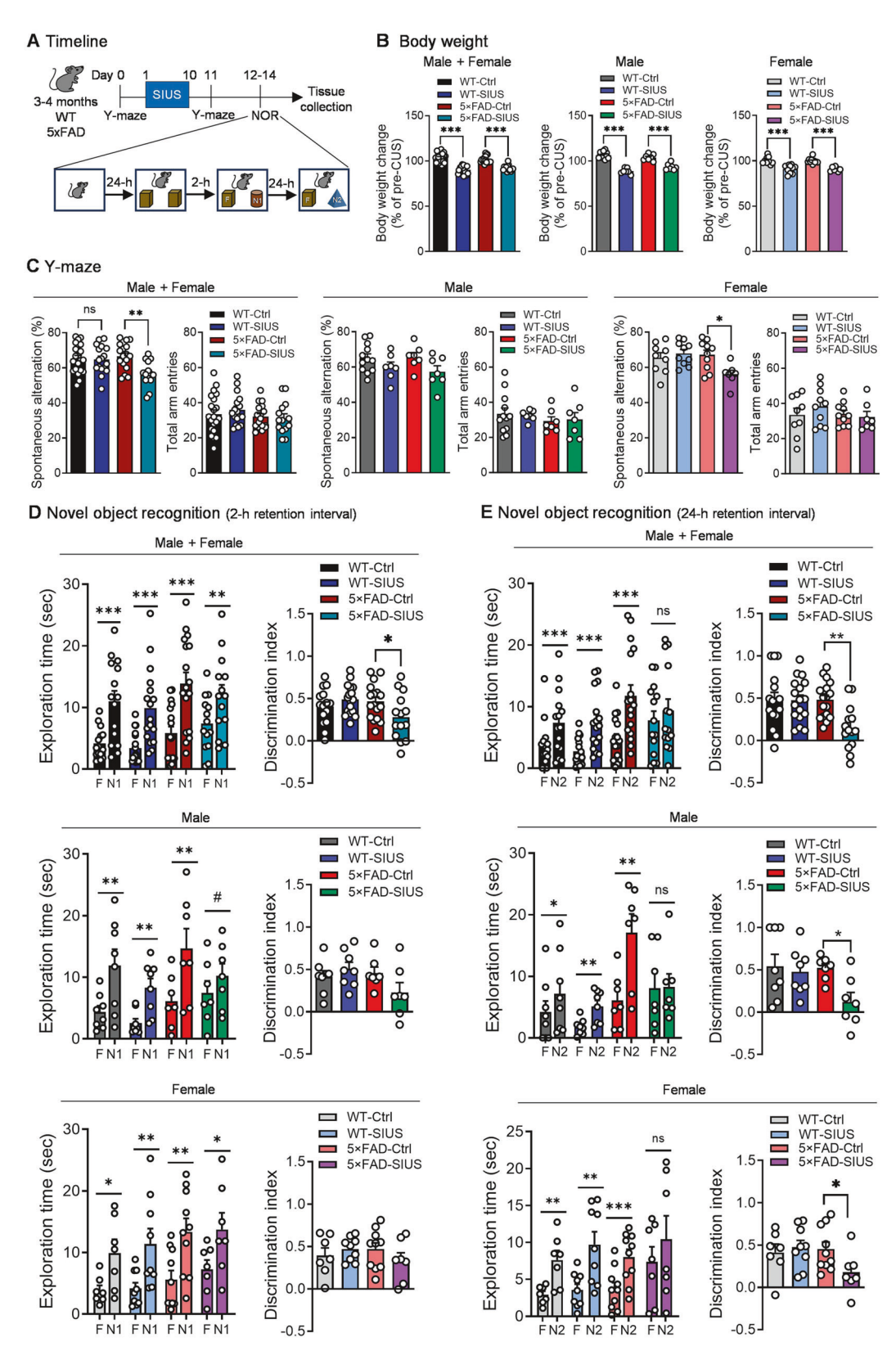


Fig. 5 Chronic social isolation-unpredictable stress induces the onset of cognition deficits in young 5xFAD mice. A Timeline of experimental procedures. **B** Body weight changes before and after exposure to 10 days of social isolation and unpredictable stress (SIUS). **C** Spontaneous alternation rate (left) and total arm entries (right) in the Y-maze test. WT-Ctrl: male, n=12, female, n=9; WT-SIUS: male, n=7, female, n=7, female,

weight in both male and female mice, and there was a significant interaction between stress and genotype observed in male mice, but not in female mice (Male: stress, $F_{(1,29)} = 130.3$, P < 0.001; genotype, $F_{(1,29)} = 0.651$, P = 0.426; stress × genotype interaction, $F_{(1,29)} = 8.706$, P = 0.006. Female: stress, $F_{(1,32)} = 55.38$, P < 0.001; genotype, $F_{(1,32)} = 0.079$, P = 0.780; stress × genotype interaction, $F_{(1,32)} = 0.017$, P = 0.897). While exposure to 10 days of social isolation and unpredictable stress can induce anhedonic and despair behaviors [27-30], this stress paradigm failed to induce significant changes in spatial working memory in young wild-type mice, as indicated by unaltered spontaneous alternation rate in the Y-maze (Fig. 5C). Consistent with our results presented above, group-housed, unstressed 5xFAD mice of both sexes at this young age exhibited normal spatial working memory, but they displayed increased susceptibility to social isolation-unpredictable stress, resulting in a reduced rate of spontaneous alternation in the Y-maze (Fig. 5C. Male + female: stress, $F_{(1,65)} = 7.605$, P = 0.008; genotype, $F_{(1,65)} = 3.191$, P = 0.079; stress × genotype interaction, $F_{(1,65)} = 6.135$, P = 0.016. Male: stress, $F_{(1,29)} = 5.726$, P = 0.023; genotype, $F_{(1,29)} = 0.131$, P = 0.720; stress × genotype interaction, $F_{(1,29)} = 0.350$, P = 0.559. Female: stress, $F_{(1,32)} = 2.799$, P = 0.104; genotype, $F_{(1,32)} = 4.081$, P = 0.052; stress × genotype interaction, $F_{(1.32)} = 7.166$, P = 0.012). Total arm entries in the Y-maze test exhibited no significant differences between two genotype groups subjected to control or chronic stress conditions (Fig. 5C. Male + female: stress, $F_{(1,65)} = 0.127$, P = 0.722; genotype. $F_{(1,65)} = 1.793,$ P = 0.185; stress × genotype interaction, $F_{(1,65)} = 0.535$, P = 0.467. Male: stress, $F_{(1,29)} = 0.0004$, P = 0.984; genotype, $F_{(1,29)} = 0.969$, P = 0.333; stress × genotype interaction, $F_{(1,29)} = 0.080$, P = 0.779. Female: stress, $F_{(1,32)} = 0.238$, P = 0.629; genotype, $F_{(1,32)} = 0.717$, P = 0.403; stress \times genotype interaction, $F_{(1,32)} = 1.039, P = 0.316$).

Subjecting young wild-type mice to 10 days of social isolation and unpredictable stress did not significantly impact short-term object recognition memory (measured after a 2-h retention interval) (Fig. 5D; male + female: wild-type-Ctrl: paired t-test, $t_{14} = 5.319$, P < 0.001; wild-type-stress: Wilcoxon matched-pairs signed rank test, P < 0.001) or long-term object recognition memory (measured after a 24-h retention interval) (Fig. 5E; male + female: wild-type-Ctrl: Wilcoxon matched-pairs signed rank test, P < 0.001; wild-type-stress: paired t-test, $t_{16} = 5.356$, P < 0.001) in the novel object recognition test. When the data were analyzed separately for male and female wild-type mice, both sexes exhibited no significant impairment in novel object recognition after exposure to 10 days of social isolation and unpredictable stress (Fig. 5D-2-h retention interval, male wildtype-Ctrl: paired t-test, $t_7 = 3.900$, P = 0.006; male wild-type-stress: Wilcoxon matched-pairs signed rank test, P = 0.008; female wildtype-Ctrl: paired t-test, $t_6 = 3.427$, P = 0.014; female wild-type-stress: paired t-test, $t_8 = 3.871$, P = 0.005. Figure 5E-24-h retention interval, male wild-type-Ctrl: paired t-test, $t_7 = 2.911$, P = 0.023; male wildtype-stress: paired t-test, $t_7 = 3.917$, P = 0.006; female wild-type-Ctrl: paired t-test, $t_6 = 3.855$, P = 0.008; female wild-type-stress: paired ttest, $t_8 = 4.270$, P = 0.003), suggesting that this stress paradigm is insufficient to induce impairment in novel object recognition in young wild-type mice. Young 5xFAD mice housed in groups under non-stress conditions or under chronic stress procedure exhibited no impairments in the novel object recognition test, displaying a normal capacity to differentiate between novel and familiar objects as assessed after retention intervals of 2 h (Fig. 5D. Male + female: 5xFAD-Ctrl: Wilcoxon matched-pairs signed rank test, P < 0.001. 5xFAD-stress: paired t-test, $t_{13} = 3.258$, P = 0.006. Male: 5xFAD-Ctrl: paired t-test, $t_6 = 3.996$, P = 0.007; 5xFAD-stress: paired t-test, $t_6 = 2.429$, P = 0.051. Female: 5xFAD-Ctrl: Wilcoxon matched-pairs signed rank test, P = 0.002; 5xFAD-stress: paired t-test, $t_6 = 2.592$, P = 0.041). Similarly, the discrimination index showed no significant main effects of stress and genotype, but a significant interaction between stress and genotype when data from male and female mice were pooled for analysis (Fig. 5D; Male + female: stress, $F_{(1,59)} = 0.837$, P = 0.364; genotype, $F_{(1,59)} = 1.788$, P = 0.186; stress \times genotype interaction, $F_{(1,59)} = 5.931$, P = 0.018. Male: stress, $F_{(1,26)} = 0.646$, P = 0.429; genotype, $F_{(1,26)} = 1.926$, P = 0.177; stress \times genotype interaction, $F_{(1,26)} = 3.639$, P = 0.068. Female: stress, $F_{(1,29)} = 0.154$, P = 0.697; genotype, $F_{(1,29)} = 0.168$, P = 0.685; stress \times genotype interaction, $F_{(1,29)} = 1.987$, P = 0.169). However, while young mice of both genotypes housed in groups under nonstress conditions retained their ability to distinguish the familiar and second novel objects after a 24-h retention interval following the training session, the young 5xFAD mice exposed to social isolation and unpredictable stress displayed impaired long-term recognition memory (Fig. 5E; male + female: 5xFAD-Ctrl: paired t-test, $t_{16} = 6.113$, P < 0.001; 5xFAD-stress: paired t-test, $t_{13} = 1.503$, P = 0.157. Male: 5xFAD-Ctrl: paired t-test, $t_6 = 5.976$, P = 0.001; 5xFAD-stress: Wilcoxon matched-pairs signed rank test, P = 0.578. Female: 5xFAD-Ctrl: paired t-test, $t_9 = 6.674$, P < 0.001; 5xFAD-stress: paired t-test, $t_6 = 1.987$, P = 0.094). Analysis of the discrimination index after a 24-h retention interval from both male and female mice revealed main effects of stress and genotype as well as a significant interaction between stress and genotype (Male + female: stress, $F_{(1,59)} = 6.147$, P = 0.016; genotype, $F_{(1,59)} = 5.768$, P = 0.020; stress × genotype interaction, $F_{(1,59)} = 5.774$, P = 0.019. Male: stress, $F_{(1,26)} = 4.534$, P = 0.043; genotype, $F_{(1,26)} = 2.965$, P = 0.097; stress \times genotype interaction, $F_{(1,26)} = 2.380$, P = 0.135. Female: stress, $F_{(1,29)} = 1.420$, P = 0.243; genotype, $F_{(1,29)} = 2.067$, P = 0.161; stress × genotype interaction, $F_{(1,29)} = 3.573$, P = 0.069). The discrimination index after a 24-h retention interval was significantly decreased in 5xFAD mice subjected to social isolation and unpredictable stress (Fig. 5E). These results suggest that social isolation and unpredictable stress compromise long-term recognition memory in young 5xFAD mice.

Exacerbation of Aβ deposition in 5xFAD mice following chronic social isolation-unpredictable stress

Chronic stress and subsequent hyperactivity of the HPA axis have been shown to exacerbate neuropathology of AD [18-26]. To investigate the effects of social isolation and unpredictable stress on AB deposition in different brain regions of 5xFAD mice, mouse brains were collected following behavioral testing described above and processed for immunostaining for AB deposition. Quantitative analysis of AB plaque deposition was performed in three brain regions, including the entorhinal cortex (EC), hippocampus and medial prefrontal cortex (mPFC). These brain regions play crucial roles in learning and memory and are affected by AD [43–45]. In the EC, the A β plaque load was quantified in its subregions, i.e. lateral EC (LEC) and medial EC (MEC) that have distinct functions and connect differentially with cortical areas and hippocampal subfields [46-48]. Exposure to chronic isolation and unpredictable stress increased AB plaque load in the LEC of both male and female 5xFAD mice (Fig. 6A; LEC: male + female: Mann Whitney test, P < 0.001; male: $t_{16} = 2.458$, P = 0.026; female: Mann Whitney test, P = 0.007) and in the MEC only in female 5xFAD mice (Fig. 6A. MEC: male + female: $t_{34} = 2.084$, P = 0.045, male: Mann Whitney test, P = 0.573, female: $t_{16} = 2.387$, P = 0.030), indicating a sex difference in AB deposition in response to stress. In the hippocampus, exposure to chronic stress increased AB plaque load in the dentate gyrus (DG) of both male and female 5xFAD mice (Fig. 6B; DG-male + female: $t_{36} = 3.169$, P = 0.003; DGmale: Mann Whitney test, P = 0.034; DG-female: $t_{18} = 2.381$, P = 0.029). In the CA1, A β deposition were increased by chronic stress in both the dorsal (dCA1) and ventral (vCA1) parts of female, but not male, 5xFAD mice (Fig. 6B; dCA1-male + female: Mann Whitney test, P = 0.009; dCA1-male: Mann Whitney test, P = 0.327; dCA1-female: $t_{18} = 4.594$, P < 0.001; vCA1-male + female: Mann Whitney test, P = 0.015; vCA1-male: $t_9 = 1.057$, P = 0.318; vCA1female Mann Whitney test, P = 0.019). In the CA3, only male 5xFAD mice showed significant increase in Aβ deposition following exposure to chronic stress (Fig. 6B; CA3-male + female:

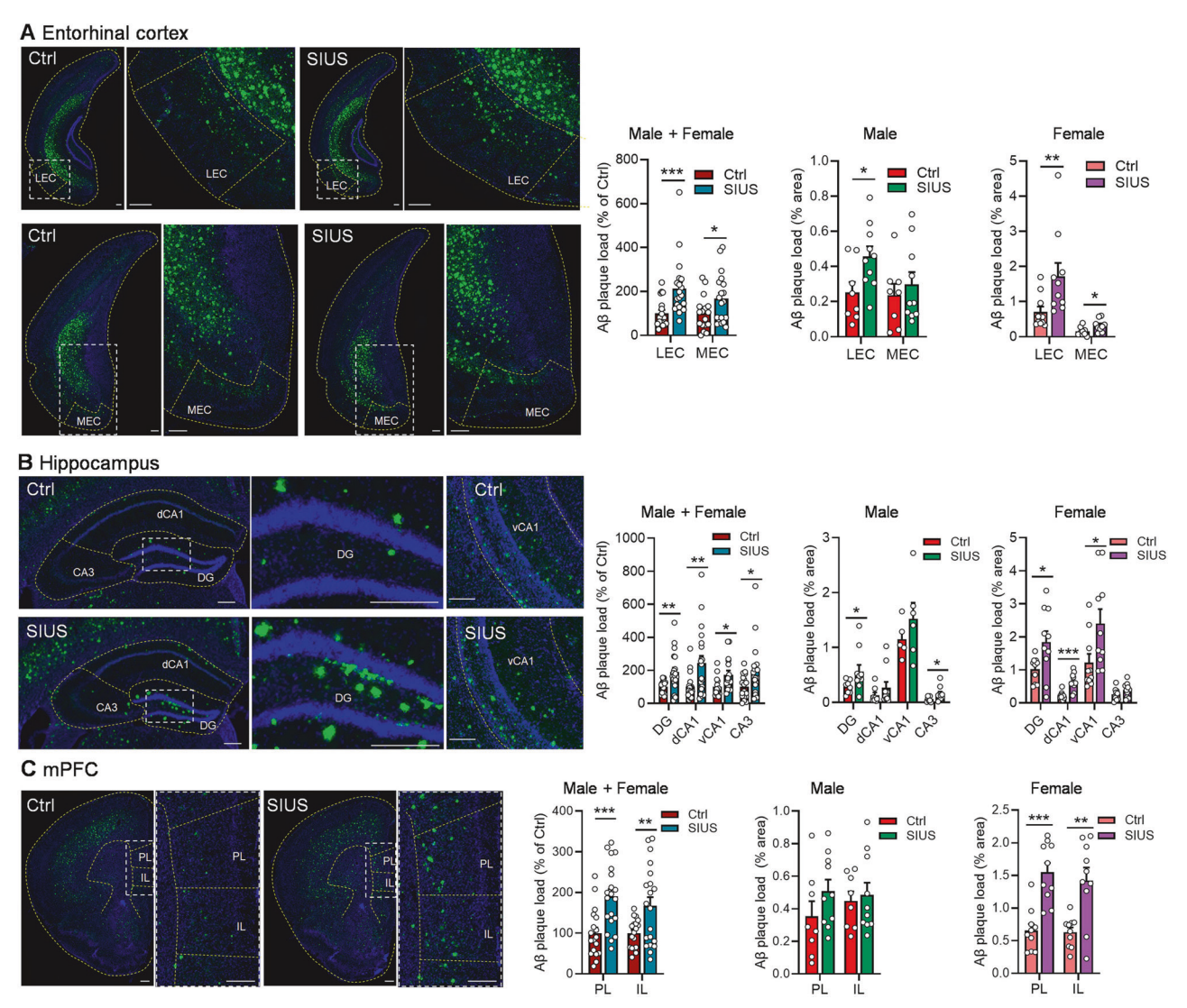


Fig. 6 Chronic social isolation-unpredictable stress accelerates Aβ plaque deposition in 5xFAD mice. Representative coronal brain sections showing staining of Aβ plaques and quantitative analysis of Aβ plaque load in the entorhinal cortex **A**, hippocampus **B** and mPFC **C** of 5xFAD mice under control (Ctrl) or chronic social isolation and unpredictable stress (SIUS) conditions. n = 8-10 sections from 4–5 mice per sex per group. Scale bar = 200 μm. *P < 0.00, **P < 0.01, ***P < 0.001 compared with Ctrl mice.

Mann Whitney test, P=0.012; CA3-male: Mann Whitney test, P=0.034; CA3-female: $t_{18}=1.502$, P=0.151). The quantification of Aβ plaque load in the mPFC was conducted in the prelimbic (PL) and infralimbic (IL) subregions. The PL and IL have similarities in cell compositions but exhibit remarkable differences in response to stress [49–51]. Increased Aβ plaque load was observed in both the PL and IL subregions of the mPFC in female 5xFAD mice exposed to chronic stress. However, no change was observed in male 5xFAD mice (Fig. 6C; PL-male + female: $t_{36}=3.900$, P<0.001; PL-male: $t_{16}=1.355$, P=0.194; PL-female: $t_{18}=5.077$, P<0.001; IL-male + female: t-test with Welch's correction, P=0.009; IL-male: $t_{16}=0.377$, P=0.711; IL-female: $t_{18}=3.778$, P=0.001). These results suggest that chronic stress exposure can exacerbate Aβ plaque burden in 5xFAD mice, but with sex differences across different brain regions.

DISCUSSION

AD is a complex and multifactorial neurodegenerative disorder. In studies using mouse models to investigate AD, both mixed genetic backgrounds and congenic genetic backgrounds have been

employed [7, 9, 15, 16]. While the utilization of mice with mixed genetic backgrounds offers the advantage of capturing a broader range of genetic variations and phenotypic traits, the inherent diversity in genetic makeup within mixed backgrounds presents a challenge when attributing observed differences solely to the manipulation of specific genes or other genetic factors. Consequently, this complexity introduces a confounder in the interpretation of phenotypic results, particularly in the case of behavioral phenotypes sensitive to both genetic variations and environmental influences. The interplay between genetic predispositions and environmental exposure can result in unique and nuanced behavioral outcomes [52, 53]. Notably, cognitive deficits, a defining trait of AD, exhibit diverse times of onset and manifestations across different AD mouse models. Even when using the same mouse model, cognitive behavioral results can vary among different laboratories [54-56]. This variability may originate from multiple factors, including genetic background, sex, age at time of testing, breeding strategies, housing conditions, and behavioral testing protocols. To minimize the confounding effects of genetic variations, congenic backgrounds are necessary for investigating the specific phenotypic consequences of transgenic expression of mutated human APP.

In this study, we analyzed age-dependent cognitive phenotypes in hemizygous transgenic 5xFAD mice on a congenic C57BL/6 J background. We found that while both male and female 5xFAD mice exhibited normal cognitive behaviors at 3-6 months of age, they developed cognitive impairments in spatial working memory, novel object recognition memory, and social recognition memory by 8-9 months. This onset of cognitive deficits is much later than what has been reported in 5xFAD mice on mixed B6/SJL backgrounds, where cognitive deficits were observed at earlier ages, between 4 and 6 months [7, 9, 57]. The onset of cognitive deficits seems to parallel AB pathology, as 5xFAD mice on congenic C57BL/6 J backgrounds show less robust AB deposition [7, 58]. Several recent studies have characterized the behavioral phenotypes of 5xFAD on the congenic C57BL/6 background [14–16]. However, in two of these studies [15, 16], only a single cognitive behavioral test was conducted to assess cognitive function, and neither study reported cognitive deficits. In the study by Forner et al. [16], they used contextual fear conditioning, a test that involves exposing mice to high levels of stress, i.e. electric shocks, to generate fear memories. While this test is effective for assessing hippocampal-dependent memory, the stress involved may potentially mask phenotypic differences. In the study by Oblak et al. [15], cognitive function was assessed using the Y-maze test. Notably, WT control mice showed a percent alternation of 49-52%, close to chance levels (50%), whereas the typical range for healthy WT mice is 60-75%. This suggests that the testing conditions in that study may not have been optimal for a reliable assessment of cognitive behavior. In the study by Locci et al. [14], the same WT control group was used for three different mutant lines (APP^{NLGF} knock-in, 5xFAD, and APP/PS1), with testing conducted at 10 months of age. Given that subtle genetic differences or drift between colonies could influence behavioral outcomes, each mutant line should have its own age-matched and concurrently tested WT control group to ensure reliable comparisons. In this study, three behavioral tests were conducted to assess distinct cognitive domains. None of these tests involve highly stressful procedures, making them well-suited for detecting baseline cognitive phenotypes. All 5xFAD mice and their WT littermate controls were tested simultaneously to ensure proper comparisons. Additionally, the inclusion of social memory assessment, a cognitive domain affected in early and middle stages of AD but less characterized in AD mouse models [14], provides new insights into the cognitive phenotypes. Our findings that 5xFAD mice exhibited normal cognitive performance at 3-6 months of age but developed cognitive deficits by 8-9 months across three behavioral tests, confirming a reliable and progressive cognitive decline with aging.

Chronic stress can exert long-lasting effects on cognitive function and contribute to the progression of AD pathology [59-61]. The impact of stress on AD-related pathology has been studied in various transgenic mouse models; however, findings have been inconsistent [62-64]. For instance, a study using 5xFAD mice on the B6/SJL hybrid background found that restraint and social isolation stress impaired fear memory and increased $A\beta_{42}$ plaque burden in the hippocampus of 3-month-old females but not males [62]. Another study reported that chronic isolation stress increased hippocampal AB plaque accumulation in male 5xFAD mice, though the genetic background was not reported [63]. Additionally, maternal separation during early postnatal development impaired novel object recognition memory in both male and female 5xFAD mice on the B6/SJL hybrid background, but only stressed females exhibited greater AB deposition in the PFC [64]. These discrepancies may be attributed to differences in genetic backgrounds, sex, stress paradigms, and behavioral tests.

In the present study, we investigated the effects of chronic stress on both cognitive behaviors and A β accumulation in young 5xFAD mice on the congenic C57BL/6 J background, using a chronic unpredictable stress paradigm well-established in our

laboratory [27–30]. This paradigm involves the application of diverse stressors to socially isolated mice at variable times and in a randomized sequence to prevent habituation and maintain a sustained stress response. This approach simulates real-life stress exposure, in which individuals face unpredictable and varied stressors over time. While exposure to this stress paradigm had no effect on young WT littermate control mice, it induced impairments in spatial working memory and long-term object recognition memory in age- and sex-matched 5xFAD mice. We observed that female 5xFAD mice were more vulnerable to the stress effects on spatial working memory, whereas both male and female 5xFAD mice exhibited similar susceptibility to stress-induced impairments in long-term object recognition memory, suggesting sexdimorphic effects. One potential mechanism underlying these observations is that AB accumulation in brain regions involved in stress responses, such as the hippocampus, amygdala, entorhinal cortex and prefrontal cortex [65], predisposes 5xFAD mice to increased stress susceptibility. These same brain regions also play central roles in cognitive processes [66-69]. This study demonstrated that exposure to chronic social isolation-unpredictable stress increased AB accumulation in the hippocampus, entorhinal cortex and prefrontal cortex. Sex differences in cognitive impairment induced by chronic stress may be attributed to differences in AB accumulation. Given the essential roles of the CA1 and mPFC in maintaining spatial working memory [70–72] and the importance of the medial entorhinal cortex in processing spatial information [73], the unaltered Aβ load in these regions in male 5xFAD mice may underlie their resilience to chronic stressinduced deficits in spatial working memory. It is proposed that the synergistic effects of AB accumulation and chronic stress exposure converge on brain regions involved in both stress responses and cognitive processes, creating a detrimental cycle that induces early-onset of cognitive impairment.

Clinical studies have established a correlation between metabolic disturbances and the development of AD pathology [74–76]. We observed AB accumulation in the pons and medulla at 4 months of age, with a progressive increase by 8 months, particularly in the PPN, PB, and NTS—regions critical for regulating feeding, thermogenesis, and energy expenditure [77, 78]. Despite this early AB accumulation, 5xFAD mice displayed normal body weight and no significant changes in overall energy metabolism at 4 months. However, by 11 months, these mice showed a decrease in body weight. Analysis of energy expenditure revealed increased oxygen consumption, CO2 production, and locomotor activity, which likely contributed to the observed weight loss. These metabolic changes may be partially mediated by progressive AB accumulation in the brainstem, including the NTS, PB and PPN. Interestingly, 5xFAD mice at both 4 and 11 months of age exhibited an increased RER during the first half of the dark cycle, suggesting increased carbohydrate utilization over lipid oxidation [79]. This shift in systemic metabolic fuel preference may impact brain glucose availability, as the brain relies on circulating glucose due to its minimal glycogen stores. Notably, reduced glucose utilization in the brain has been reported in aged APP mouse models [80, 81], supporting a link between Aβ pathology and metabolic dysfunction. While chronic social isolation and unpredictable stress reduced body weight in young 5xFAD mice, it remains unclear whether this stress paradigm triggers other metabolic alterations. In WT C57BL/6 J mice, this stress paradigm was observed to reduce body weight and locomotor activity while increasing RER during the first half of the dark phase (unpublished data). Future studies will investigate whether chronic stress exacerbates metabolic dysfunction in 5xFAD mice.

Chronic stress induces prolonged HPA axis activation, leading to excessive glucocorticoid secretion, which can impair cognitive function and exacerbate A β plaque formation. Administration of glucocorticoids has been shown to increase APP expression and β -site APP-cleaving enzyme 1 (BACE1), the latter of which cleaves

APP to initiate the production of AB peptides [23, 25]. Furthermore, cortisol levels have been linked to the progression of dementia [82-84]. Increased peripheral and central nervous system cortisol levels have been reported in AD [82, 84, 85], and activation of the HPA axis during the early stages of AD pathology may precede cognitive impairment [86]. In addition to the direct effects of glucocorticoids on AB production, chronic stress may influence specific neuronal populations that are upstream of brain regions affected by AB pathology. For instance, the hypothalamus plays a crucial role in regulating the HPA axis [87-89]; however, in 5xFAD mice, it exhibits low levels of Aβ deposition. Nonetheless, chronic stress may alter neuronal activity in this region [30], leading to prolonged HPA activation [90]. Chronic HPA hyperactivation and elevated glucocorticoid levels have been linked to metabolic disorders, which may, in turn, exacerbate AD-related pathology and cognitive impairment.

These studies underscore the intricate relationship between genetic vulnerability, aging, and stress. Genetic predispositions, such as those present in 5xFAD mice, drive early amyloid pathology, while aging introduces additional molecular and cellular changes that exacerbate neurodegeneration and cognitive decline. Chronic stress, through persistent HPA axis activation or neural mechanisms, accelerates brain aging and further worsens neuropathology and cognitive deficits. The convergence of these risk factors shapes the trajectory of AD-related phenotypes. Understanding these interactions is needed for identifying therapeutic targets that could mitigate the combined effects of genetic risk, aging, and chronic stress on AD progression. Future studies will explore whether interventions or manipulations that modulate stress responses can alter disease outcomes and enhance cognitive resilience in AD.

DATA AVAILABILITY

The datasets generated during the current study are available from the corresponding authors upon request.

REFERENCES

- Alzheimer's Association. 2024 Alzheimer's disease facts and figures. Alzheimers Dement 2024;20:3708–821.
- Chartier-Harlin MC, Crawford F, Houlden H, Warren A, Hughes D, Fidani L, et al. Early-onset Alzheimer's disease caused by mutations at codon 717 of the betaamyloid precursor protein gene. Nature. 1991;353:844–6.
- Goate A, Chartier-Harlin MC, Mullan M, Brown J, Crawford F, Fidani L, et al. Segregation of a missense mutation in the amyloid precursor protein gene with familial Alzheimer's disease. Nature. 1991;349:704–6.
- Sherrington R, Rogaev EI, Liang Y, Rogaeva EA, Levesque G, Ikeda M, et al. Cloning
 of a gene bearing missense mutations in early-onset familial Alzheimer's disease.
 Nature. 1995;375:754–60.
- Rogaev El, Sherrington R, Rogaeva EA, Levesque G, Ikeda M, Liang Y, et al. Familial Alzheimer's disease in kindreds with missense mutations in a gene on chromosome 1 related to the Alzheimer's disease type 3 gene. Nature. 1995;376:775–8.
- Sherrington R, Froelich S, Sorbi S, Campion D, Chi H, Rogaeva EA, et al. Alzheimer's disease associated with mutations in presenilin 2 is rare and variably penetrant. Hum Mol Genet. 1996;5:985–8.
- Oakley H, Cole SL, Logan S, Maus E, Shao P, Craft J, et al. Intraneuronal betaamyloid aggregates, neurodegeneration, and neuron loss in transgenic mice with five familial Alzheimer's disease mutations: potential factors in amyloid plaque formation. J Neurosci. 2006;26:10129–40.
- 8. Chang B, Hawes NL, Hurd RE, Davisson MT, Nusinowitz S, Heckenlively JR. Retinal degeneration mutants in the mouse. Vision Res. 2002;42:517–25.
- Ohno M, Chang L, Tseng W, Oakley H, Citron M, Klein WL, et al. Temporal memory deficits in Alzheimer's mouse models: rescue by genetic deletion of BACE1. Eur J Neurosci. 2006;23:251–60.
- Duncan MJ, Farlow H, Tirumalaraju C, Yun DH, Wang C, Howard JA, et al. Effects of the dual orexin receptor antagonist DORA-22 on sleep in 5XFAD mice. Alzheimers Dement. 2019;5:70–80.
- Sadleir KR, Popovic J, Khatri A, Vassar R. Oral nimodipine treatment has no effect on amyloid pathology or neuritic dystrophy in the 5XFAD mouse model of amyloidosis. PLoS ONE. 2022;17:e0263332.

- Qosa H, Kaddoumi A. Effect of mouse strain as a background for Alzheimer's disease models on the clearance of amyloid-beta. J Syst Integr Neurosci. 2016;2:135–40.
- Ammassari-Teule M. Inbred mice again at stake: how the cognitive profile of the wild-type mouse background discloses pathogenic effects of APP mutations. Front Behav Neurosci. 2022;16:868473.
- Locci A, Orellana H, Rodriguez G, Gottliebson M, McClarty B, Dominguez S, et al. Comparison of memory, affective behavior, and neuropathology in APP(NLGF) knock-in mice to 5xFAD and APP/PS1 mice. Behav Brain Res. 2021;404:113192.
- Oblak AL, Lin PB, Kotredes KP, Pandey RS, Garceau D, Williams HM, et al. Comprehensive evaluation of the 5XFAD mouse model for preclinical testing applications: a MODEL-AD study. Front Aging Neurosci. 2021;13:713726.
- Forner S, Kawauchi S, Balderrama-Gutierrez G, Kramar EA, Matheos DP, Phan J, et al. Systematic phenotyping and characterization of the 5xFAD mouse model of Alzheimer's disease. Sci Data. 2021;8:270.
- Dubois B, Villain N, Frisoni GB, Rabinovici GD, Sabbagh M, Cappa S, et al. Clinical diagnosis of Alzheimer's disease: recommendations of the international working group. Lancet Neurol. 2021;20:484–96.
- Rothman SM, Herdener N, Camandola S, Texel SJ, Mughal MR, Cong WN, et al. 3xTgAD mice exhibit altered behavior and elevated Abeta after chronic mild social stress. Neurobiol Aging. 2012;33:830 e831–812.
- Carroll JC, Iba M, Bangasser DA, Valentino RJ, James MJ, Brunden KR, et al. Chronic stress exacerbates tau pathology, neurodegeneration, and cognitive performance through a corticotropin-releasing factor receptor-dependent mechanism in a transgenic mouse model of tauopathy. J Neurosci. 2011;31:14436-49.
- Dong H, Goico B, Martin M, Csernansky CA, Bertchume A, Csernansky JG. Modulation of hippocampal cell proliferation, memory, and amyloid plaque deposition in APPsw (Tg2576) mutant mice by isolation stress. Neuroscience. 2004;127:601–9.
- Baglietto-Vargas D, Chen Y, Suh D, Ager RR, Rodriguez-Ortiz CJ, Medeiros R, et al. Short-term modern life-like stress exacerbates Abeta-pathology and synapse loss in 3xTq-AD mice. J Neurochem. 2015;134:915–26.
- Elliott EM, Mattson MP, Vanderklish P, Lynch G, Chang I, Sapolsky RM. Corticosterone exacerbates kainate-induced alterations in hippocampal tau immunoreactivity and spectrin proteolysis in vivo. J Neurochem. 1993;61:57–67.
- Green KN, Billings LM, Roozendaal B, McGaugh JL, LaFerla FM. Glucocorticoids increase amyloid-beta and tau pathology in a mouse model of Alzheimer's disease. J Neurosci. 2006;26:9047–56.
- Sotiropoulos I, Catania C, Pinto LG, Silva R, Pollerberg GE, Takashima A, et al. Stress acts cumulatively to precipitate Alzheimer's disease-like tau pathology and cognitive deficits. J Neurosci. 2011;31:7840–7.
- Wang Y, Li M, Tang J, Song M, Xu X, Xiong J, et al. Glucocorticoids facilitate astrocytic amyloid-beta peptide deposition by increasing the expression of APP and BACE1 and decreasing the expression of amyloid-beta-degrading proteases. Endocrinology. 2011;152:2704–15.
- Joshi YB, Chu J, Pratico D. Stress hormone leads to memory deficits and altered tau phosphorylation in a model of Alzheimer's disease. J Alzheimers Dis. 2012;31:167–76.
- Lei Y, Wang J, Wang D, Li C, Liu B, Fang X, et al. SIRT1 in forebrain excitatory neurons produces sexually dimorphic effects on depression-related behaviors and modulates neuronal excitability and synaptic transmission in the medial prefrontal cortex. Mol Psychiatry. 2020;25:1094–111.
- Lei Y, Wang D, Bai Y, Nougaisse J, Weintraub NL, Guo M, et al. Leptin enhances social motivation and reverses chronic unpredictable stress-induced social anhedonia during adolescence. Mol Psychiatry. 2022;27:4948–58.
- Fang X, Jiang S, Wang J, Bai Y, Kim CS, Blake D, et al. Chronic unpredictable stress induces depression-related behaviors by suppressing AgRP neuron activity. Mol Psychiatry. 2021;26:2299–315.
- Fang X, Chen Y, Wang J, Zhang Z, Bai Y, Denney K, et al. Increased intrinsic and synaptic excitability of hypothalamic POMC neurons underlies chronic stressinduced behavioral deficits. Mol Psychiatry. 2023;28:1365–82.
- Hsiao K, Chapman P, Nilsen S, Eckman C, Harigaya Y, Younkin S, et al. Correlative memory deficits, Abeta elevation, and amyloid plaques in transgenic mice. Science. 1996;274:99–102.
- 32. Ennaceur A, Delacour J. A new one-trial test for neurobiological studies of memory in rats. 1: behavioral data. Behav Brain Res. 1988;31:47–59.
- Ennaceur A. One-trial object recognition in rats and mice: methodological and theoretical issues. Behav Brain Res. 2010;215:244–54.
- 34. Leger M, Quiedeville A, Bouet V, Haelewyn B, Boulouard M, Schumann-Bard P, et al. Object recognition test in mice. Nat Protoc. 2013;8:2531–7.
- Schindelin J, Arganda-Carreras I, Frise E, Kaynig V, Longair M, Pietzsch T, et al. Fiji: an open-source platform for biological-image analysis. Nat Methods. 2012;9:676–82.
- Maarouf CL, Kokjohn TA, Whiteside CM, Macias MP, Kalback WM, Sabbagh MN, et al. Molecular differences and similarities between Alzheimer's disease and the 5XFAD transgenic mouse model of amyloidosis. Biochem Insights. 2013;6:1–10.

4734

- Liebmann T, Renier N, Bettayeb K, Greengard P, Tessier-Lavigne M, Flajolet M. Three-dimensional study of Alzheimer's disease hallmarks using the iDISCO clearing method. Cell Rep. 2016;16:1138–52.
- Renier N, Wu Z, Simon DJ, Yang J, Ariel P, Tessier-Lavigne M. iDISCO: a simple, rapid method to immunolabel large tissue samples for volume imaging. Cell. 2014;159:896–910.
- Stranahan AM, Tabet A, Anikeeva P. Region-specific targeting of microglia in vivo using direct delivery of tamoxifen metabolites via microfluidic polymer fibers. Brain Behav Immun. 2024;115:131–42.
- 40. Bria A, lannello G. TeraStitcher a tool for fast automatic 3D-stitching of teravoxel-sized microscopy images. BMC Bioinformatics. 2012;13:316.
- Bay H, Ess A, Tuytelaars T, Van Gool L. Speeded-Up robust features (SURF). Comput Vis Image Und. 2008;110:346–59.
- 42. Antunes M, Biala G. The novel object recognition memory: neurobiology, test procedure, and its modifications. Cogn Process. 2012;13:93–110.
- Rao YL, Ganaraja B, Murlimanju BV, Joy T, Krishnamurthy A, Agrawal A. Hippocampus and its involvement in Alzheimer's disease: a review. 3 Biotech. 2022:12:55.
- Igarashi KM. Entorhinal cortex dysfunction in Alzheimer's disease. Trends Neurosci. 2023;46:124–36.
- 45. Jobson DD, Hase Y, Clarkson AN, Kalaria RN. The role of the medial prefrontal cortex in cognition, ageing and dementia. Brain Commun. 2021;3:fcab125.
- Grienberger C, Magee JC. Entorhinal cortex directs learning-related changes in CA1 representations. Nature. 2022;611:554–62.
- 47. Maass A, Berron D, Libby LA, Ranganath C, Duzel E. Functional subregions of the human entorhinal cortex. eLife. 2015;4:e06426.
- Knierim JJ, Neunuebel JP, Deshmukh SS. Functional correlates of the lateral and medial entorhinal cortex: objects, path integration and local-global reference frames. Philos Trans R Soc Lond B Biol Sci. 2014;369:20130369.
- Oliveira LA, Carvalho II, Kurokawa RY, Duarte JO, Busnardo C, Crestani CC. Differential roles of prelimbic and infralimbic cholinergic neurotransmissions in control of cardiovascular responses to restraint stress in rats. Brain Res Bull. 2022;181:175–82.
- Porter JT, Sepulveda-Orengo MT. Learning-induced intrinsic and synaptic plasticity in the rodent medial prefrontal cortex. Neurobiol Learn Mem. 2020;169: 107117.
- Laine MA, Greiner EM, Shansky RM. Sex differences in the rodent medial prefrontal cortex - what do and don't we know? Neuropharmacology. 2024;248: 109867
- Kas MJ, Fernandes C, Schalkwyk LC, Collier DA. Genetics of behavioural domains across the neuropsychiatric spectrum; of mice and men. Mol Psychiatry. 2007;12:324–30.
- Rutter M, Moffitt TE, Caspi A. Gene-environment interplay and psychopathology: multiple varieties but real effects. J Child Psychol Psychiatry. 2006;47:226–61.
- Jankowsky JL, Zheng H. Practical considerations for choosing a mouse model of Alzheimer's disease. Mol Neurodegener. 2017;12:89.
- Zhong MZ, Peng T, Duarte ML, Wang M, Cai D. Updates on mouse models of Alzheimer's disease. Mol Neurodegener. 2024;19:23.
- Padua MS, Guil-Guerrero JL, Lopes PA. Behaviour hallmarks in Alzheimer's disease 5xFAD mouse model. Int J Mol Sci. 2024;25:6766.
- Devi L, Ohno M. Mitochondrial dysfunction and accumulation of the betasecretase-cleaved C-terminal fragment of APP in Alzheimer's disease transgenic mice. Neurobiol Dis. 2012:45:417–24.
- Gail Canter R, Huang WC, Choi H, Wang J, Ashley Watson L, Yao CG, et al. 3D mapping reveals network-specific amyloid progression and subcortical susceptibility in mice. Commun Biol. 2019;2:360.
- McEwen BS. Physiology and neurobiology of stress and adaptation: central role of the brain. Physiol Rev. 2007;87:873–904.
- Lyons CE, Bartolomucci A. Stress and Alzheimer's disease: a senescence link? Neurosci Biobehav Rev. 2020;115:285–98.
- Justice NJ. The relationship between stress and Alzheimer's disease. Neurobiol Stress. 2018;8:127–33.
- Devi L, Alldred MJ, Ginsberg SD, Ohno M. Sex- and brain region-specific acceleration of beta-amyloidogenesis following behavioral stress in a mouse model of Alzheimer's disease. Mol Brain. 2010;3:34.
- Peterman JL, White JD, Calcagno A, Hagen C, Quiring M, Paulhus K, et al. Prolonged isolation stress accelerates the onset of Alzheimer's disease-related pathology in 5xFAD mice despite running wheels and environmental enrichment. Behav Brain Res. 2020:379:112366.
- Bachiller S, Hidalgo I, Garcia MG, Boza-Serrano A, Paulus A, Denis Q, et al. Early-life stress elicits peripheral and brain immune activation differently in wild type and 5xFAD mice in a sex-specific manner. J Neuroinflammation. 2022;19:151.
- McEwen BS, Nasca C, Gray JD. Stress effects on neuronal structure: hippocampus, amygdala, and prefrontal cortex. Neuropsychopharmacology. 2016;41:3–23.
- Yadav N, Toader A, Rajasethupathy P. Beyond hippocampus: thalamic and prefrontal contributions to an evolving memory. Neuron. 2024;112:1045–59.

- Sigurdsson T, Duvarci S. Hippocampal-prefrontal interactions in cognition, behavior and psychiatric disease. Front Syst Neurosci. 2015;9:190.
- Lisman J, Buzsaki G, Eichenbaum H, Nadel L, Ranganath C, Redish AD. Viewpoints: how the hippocampus contributes to memory, navigation and cognition. Nat Neurosci. 2017;20:1434–47.
- Gerlei KZ, Brown CM, Surmeli G, Nolan MF. Deep entorhinal cortex: from circuit organization to spatial cognition and memory. Trends Neurosci. 2021;44:876–87.
- Dillon GM, Qu X, Marcus JN, Dodart JC. Excitotoxic lesions restricted to the dorsal CA1 field of the hippocampus impair spatial memory and extinction learning in C57BL/6 mice. Neurobiol Learn Mem. 2008;90:426–33.
- Vogel P, Hahn J, Duvarci S, Sigurdsson T. Prefrontal pyramidal neurons are critical for all phases of working memory. Cell Rep. 2022;39:110659.
- Bygrave AM, Jahans-Price T, Wolff AR, Sprengel R, Kullmann DM, Bannerman DM, et al. Hippocampal-prefrontal coherence mediates working memory and selective attention at distinct frequency bands and provides a causal link between schizophrenia and its risk gene GRIA1. Transl Psychiatry. 2019;9:142.
- Van Cauter T, Camon J, Alvernhe A, Elduayen C, Sargolini F, Save E. Distinct roles of medial and lateral entorhinal cortex in spatial cognition. Cereb Cortex. 2013;23:451–9.
- Vidoni ED, Townley RA, Honea RA, Burns JM, Alzheimer's Disease Neuroimaging I. Alzheimer disease biomarkers are associated with body mass index. Neurology. 2011;77:1913–20.
- Gu Y, Scarmeas N, Cosentino S, Brandt J, Albert M, Blacker D, et al. Change in body mass index before and after Alzheimer's disease onset. Curr Alzheimer Res. 2014:11:349–56.
- Cova I, Clerici F, Rossi A, Cucumo V, Ghiretti R, Maggiore L, et al. Weight loss predicts progression of mild cognitive impairment to Alzheimer's disease. PLoS ONE. 2016;11:e0151710.
- Grill HJ, Hayes MR. Hindbrain neurons as an essential hub in the neuroanatomically distributed control of energy balance. Cell Metab. 2012;16:296–309.
- Arcon M. The interplay between hypothalamic and brainstem nuclei in homeostatic control of energy balance. Behav Brain Res. 2025;480:115398.
- Simonson DC, DeFronzo RA. Indirect calorimetry: methodological and interpretative problems. Am J Physiol. 1990;258:E399–412.
- Huang J, van Zijl PCM, Han X, Dong CM, Cheng GWY, Tse KH, et al. Altered d-glucose in brain parenchyma and cerebrospinal fluid of early Alzheimer's disease detected by dynamic glucose-enhanced MRI. Sci Adv. 2020;6:eaba3884.
- Kumar V, Kim SH, Bishayee K. Dysfunctional glucose metabolism in Alzheimer's disease onset and potential pharmacological interventions. Int J Mol Sci. 2022;23:9540.
- Csernansky JG, Dong H, Fagan AM, Wang L, Xiong C, Holtzman DM, et al. Plasma cortisol and progression of dementia in subjects with Alzheimer-type dementia. Am J Psychiatry. 2006:163:2164–9.
- Peavy GM, Lange KL, Salmon DP, Patterson TL, Goldman S, Gamst AC, et al. The
 effects of prolonged stress and APOE genotype on memory and cortisol in older
 adults. Biol Psychiatry. 2007;62:472–8.
- Pietrzak RH, Laws SM, Lim YY, Bender SJ, Porter T, Doecke J, et al. Plasma cortisol, brain amyloid-beta, and cognitive decline in preclinical Alzheimer's disease: a 6-year prospective cohort study. Biol Psychiatry Cogn Neurosci Neuroimaging. 2017;2:45–52.
- Popp J, Wolfsgruber S, Heuser I, Peters O, Hull M, Schroder J, et al. Cerebrospinal fluid cortisol and clinical disease progression in MCl and dementia of Alzheimer's type. Neurobiol Aging. 2015;36:601–7.
- Hebda-Bauer EK, Simmons TA, Sugg A, Ural E, Stewart JA, Beals JL, et al. 3xTg-AD mice exhibit an activated central stress axis during early-stage pathology. J Alzheimers Dis. 2013;33:407–22.
- Herman JP, McKlveen JM, Ghosal S, Kopp B, Wulsin A, Makinson R, et al. Regulation of the hypothalamic-pituitary-adrenocortical stress response. Compr Physiol. 2016:6:603–21.
- Herman JP, Cullinan WE. Neurocircuitry of stress: central control of the hypothalamo-pituitary-adrenocortical axis. Trends Neurosci. 1997;20:78–84.
- Jacobson L, Sapolsky R. The role of the hippocampus in feedback regulation of the hypothalamic-pituitary-adrenocortical axis. Endocr Rev. 1991;12:118–34.
- Lu XY, Barsh GS, Akil H, Watson SJ. Interaction between alpha-melanocytestimulating hormone and corticotropin-releasing hormone in the regulation of feeding and hypothalamo-pituitary-adrenal responses. J Neurosci. 2003;23:7863–72.
- 91. Franklin KB. The mouse brain in stereotaxic coordinates. San Diego: Academic Press; 2001.

AUTHOR CONTRIBUTIONS

XYL and YL designed and directed the project. YL, JN, MM and YB performed the experiments and collected the data. MMM and KD assisted with mouse breeding and genotyping. AMS and JCG conducted brain tissue clearing, staining, 3-D imaging, image processing and quantification. QD supervised confocal microscopy and contributed to discussion. XYL and YL analyzed the data, prepared the figures and wrote the paper with input from all authors.

FUNDING

This work was supported by grants from the NIH (AG083841, AG062166, AG064895 and AG076235).

COMPETING INTERESTS

The authors declare no competing interests.

ETHICS APPROVAL

All animal procedures were approved by the Institutional Animal Care and Use Committee of Augusta University (Animal Use Protocol #2017-0868) and conducted in accordance with the NIH Guide for the Care and Use of Laboratory Animals.

ADDITIONAL INFORMATION

Correspondence and requests for materials should be addressed to Yun Lei or Xin-Yun Lu.

Reprints and permission information is available at http://www.nature.com/reprints

Publisher's note Springer Nature remains neutral with regard to jurisdictional claims in published maps and institutional affiliations.

Open Access This article is licensed under a Creative Commons Attribution-NonCommercial-NoDerivatives 4.0 International License,

which permits any non-commercial use, sharing, distribution and reproduction in any medium or format, as long as you give appropriate credit to the original author(s) and the source, provide a link to the Creative Commons licence, and indicate if you modified the licensed material. You do not have permission under this licence to share adapted material derived from this article or parts of it. The images or other third party material in this article are included in the article's Creative Commons licence, unless indicated otherwise in a credit line to the material. If material is not included in the article's Creative Commons licence and your intended use is not permitted by statutory regulation or exceeds the permitted use, you will need to obtain permission directly from the copyright holder. To view a copy of this licence, visit http://creativecommons.org/licenses/by-nc-nd/4.0/.

© The Author(s) 2025